How good are the internal conversion coefficients now?

S. Raman,* C. W. Nestor, Jr., A. Ichihara,† and M. B. Trzhaskovskaya‡
Oak Ridge National Laboratory, Oak Ridge, Tennessee 37831
(Received 30 May 2002; published 29 October 2002)

To fully utilize experimental internal conversion coefficients, one needs a reliable calculation of theoretical values. We have assembled a set of 100 experimental conversion coefficients, 45 α_K and 55 α_T values, measured with an accuracy of better than 5%, and generated the corresponding theoretical values using two methods, relativistic Hartree-Fock-Slater (RHFS) and relativistic Dirac-Fock (DF). Extensive comparisons of the experimental values with the two sets of theoretical values show that the DF method is clearly superior to the RHFS method in the overall reproduction of the experimental internal conversion coefficients. We discuss in some detail the differences between various versions of these two theoretical approaches, with a view to understanding which of these differences are most critical to obtaining agreement with experiment.

DOI: 10.1103/PhysRevC.66.044312 PACS number(s): 23.20.Nx, 33.50.−j

I. INTRODUCTION

The internal conversion process (ICP) is used extensively in solving many problems of nuclear physics. Through comparison of experimental internal conversion coefficients (ICCs) [measured for different atomic shells ($\alpha_K, \alpha_{L_1}, \ldots$) or for all shells combined (α_T)] with the corresponding theoretical values, multipolarities and mixing ratios of nuclear transitions are determined. These are used for (i) assignment of spins and parities for nuclear levels, (ii) elaboration of level schemes and nuclear decay schemes, and (iii) checking the balance of transition intensities—that is, in the end, to test and refine various nuclear structure models. Moreover, ICP data have applications in interdisciplinary investigations such as Mössbauer experiments, studies of the electronic structure of condensed matter, etc.

For an analysis of experiments involving ICC measurements, theoretical ICCs are required. The more accurate are the ICC calculations, the more reliable will be the conclusions about nuclear properties. Deviation of an experimental ICC value from the theoretical value is expected only in the special case that a nuclear transition under consideration is strongly hindered.

There is a long history of generation and improvements of theoretical ICCs. Currently the most widely used ICC tables are those by Hager and Seltzer (HS) [1], Rösel, Fries, Alder, and Pauli (RFAP) [2], and Band and Trzhaskovskaya (BT) [3], all based on calculations using the relativistic Hartree-Fock-Slater (RHFS) method.

Uncertainties in the theoretical ICCs can arise from (i) details of the physical assumptions, (ii) inadequate knowledge of some quantities involved in the computations, and (iii) approximations made in the code. These sources of uncertainties have been discussed by several authors including most recently by Ryšavý and Dragoun [4]. The combined effect of these uncertainties is not known at the present time and can only be estimated by resorting to experiment.

During the 1965 Nashville Conference on ICPs [5]— the first major international conference devoted to this subject—comparison between theoretical and experimental ICCs was a recurring theme. At that time, experimenters had access to ICCs computed by Rose [6] and by Sliv and Band [7]. The available experimental α_K and α_T values carried uncertainties in the 5–10 % range. There was a convergence of evidence that theory and experiment agreed within this uncertainty range and that the theory was good enough for the ''classical'' use of ICC for determination of multipolarities and, hence, of spins and parities. Some L subshell ratios (for $E2$ transitions) differed from theory by up to 20%, but further work has removed this discrepancy.

In 1973, Raman *et al.* [8] measured the total ICC (α_T) for the 156.0-keV $M4$ transition in ^{117}Sn to an accuracy of 0.5%. Even after three decades, this measurement remains the most accurate and well-documented benchmark measurement. The measured value, $\alpha_T = 46.40 \pm 0.25$, is $\sim 3\%$ lower than the HS value of 47.8. This discrepancy prompted these authors to examine the literature for all $E3$ and $M4$ transitions whose ICCs (α_K or α_T) had been experimentally determined to better than 5% accuracy. They found five such $E3$ and ten such $M4$ transitions for which a total of 19 ICCs (14 α_K and 5 α_T values) were available. On the one hand, Raman *et al.* [8] found that experimental ICCs as small as $\alpha_K(E3) = 0.0472$ in ^{75}As and as large as $\alpha_T(M4) = 1076$ in ^{123}Te were correctly predicted by theory; on the other, the agreement between theory and experiment could be considered satisfactory were it not for the fact that the HS theoretical values for these high-multipolarity transitions were *systematically* 2–3 % larger than measured values (see Fig. 1). The clear implication was that whatever problems existed in the calculations were potentially traceable and fixable. For example, Campbell and Martin [9] were able to reduce the discrepancy, on average, to $\sim 1\%$ (for one $E3$ and nine $M4$ transitions) by using the Rosen-Lindgren exchange instead of the Kohn exchange used by Hager and Seltzer [1].

*Email address: raman@mail.phy.ornl.gov
†Permanent address: Japan Atomic Energy Research Institute, Tokai-mura, Ibaraki-ken 319-1112, Japan.
‡Permanent address: Petersburg Nuclear Physics Institute, Gatchina RU-188300, Russia.

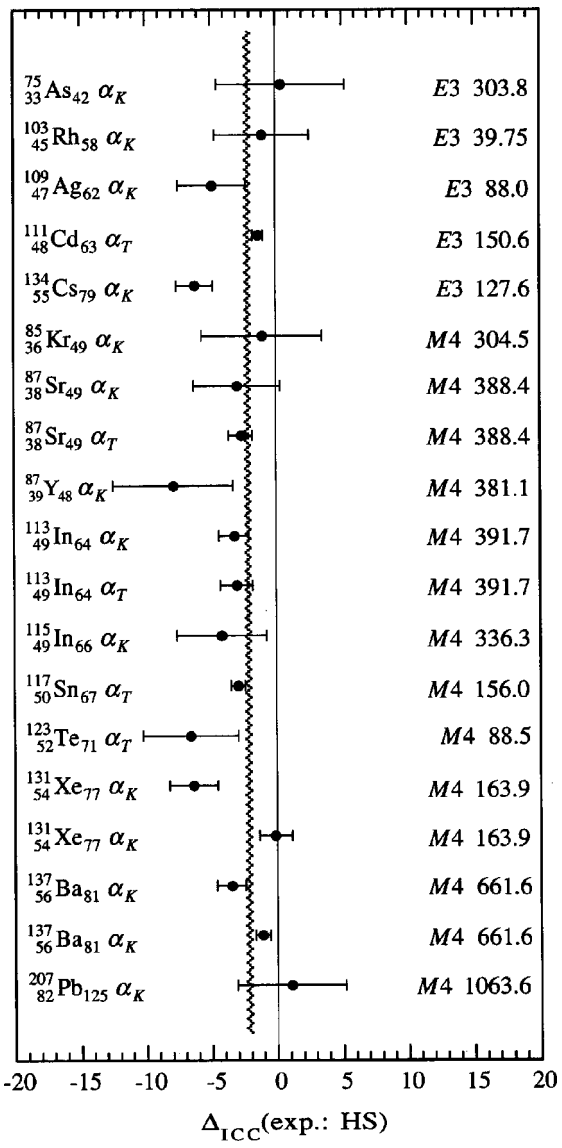

FIG. 1. Original observation made by Raman *et al.* [8] that the precisely measured $E3$ and $M4$ conversion coefficients are systematically lower than the theoretical Hager and Seltzer (HS) values. See Eq. (21) for the definition of Δ_{ICC}. The average difference is $(-2.12\pm0.23)\%$ for these 19 data points.

The systematic discrepancy problem raised by Raman *et al.* [8] was not taken seriously by most theorists who were then engaged in ICC calculations. Band and Listengarten [10] insisted that the discrepancies, if they existed at all, were not systematic and could be explained in most cases by nuclear structure effects. After carrying out some precise ICC measurements and comparing the results with theory, Dragoun *et al.* [11] endorsed this same viewpoint. A few years later, in the course of generating new tables of ICCs using the RHFS method, neither Rösel *et al.* [2] nor Band and Trzhaskovskaya [3] made any attempt to compare their ICCs with experimental values.

Another, albeit more indirect, method of obtaining experimental ICCs is to compare experimental $B(E2;0_1^+\rightarrow2_1^+)$ [abbreviated as $B(E2)\uparrow$] measurements with independently obtained half-life ($T_{1/2}$) measurements. Using this method, Raman *et al.* [12] found it necessary to reduce the HS values of α_T for $E2$ transitions by 1.5% in order to reconcile the $B(E2)\uparrow$ and $T_{1/2}$ values (see Fig. 1 of Ref. [12] and Sec. III). In a series of papers [13–15], Németh and co-workers (i) expanded the list of accurately measured ICCs ($E3$, $M3$, $E4$, and $M4$) to 64, (ii) confirmed that the HS values were indeed 2–3 % larger than experiment as found earlier by Raman *et al.* [8], and (iii) showed that the RFAP values were similarly $\sim$2.5% larger than experiment. Moreover, Band *et al.* [16–18] began comparing the BT values with experiment. They concluded that the BT values were also $\sim$3% larger than experiment.

A new ICC table has been generated recently by Band, Trzhaskovskaya, Nestor, Tikkanen, and Raman (BTNTR) [19] using a slightly modified version of the RAINE computer code [20–22]. The calculations in this case are based on the relativistic Dirac-Fock (DF) method in which the exchange interactions between bound electrons and between these electrons and the free electron receding to infinity during the conversion process are treated exactly. The exchange interaction was treated approximately in the RFHS method. There are preliminary indications [16–18,23–26] that the DF method gives results that are closer to the experimental data than those obtained with the RHFS method. A more detailed analysis with complete documentation of the experimental data is presented in this paper. The adopted ICCs for transitions occurring throughout the periodic table have also been compared with all available theoretical values. We have also examined the physical assumptions underlying these calculations and the magnitudes of the associated influences.

II. ABBREVIATIONS

We have assembled in one place the abbreviations used in this paper.

BT—Band and Trzhaskovskaya table [3],
BTNTR—Band, Trzhaskovskaya, Nestor, Tikkanen, and Raman table [19],
DF—Dirac-Fock method,
HS—Hager and Seltzer table [1],
ICC—internal conversion coefficient,
ICP—internal conversion process,
NP—no-penetration model of Rose [6],
RFAP—Rösel, Fries, Alder, and Pauli table [2],
RHFS—relativistic Hartree–Fock–Slater method,
RHFS1—RHFS with $C=1$ in Eq. (17),
RHFS $\frac{2}{3}$—RHFS with $C=\frac{2}{3}$ in Eq. (17),
RNIT—this work; Raman, Nestor, Ichihara, and Trzhaskovskaya table,
RNIT(1)—this work; self-consistent calculation (see Sec. IV B 2),
RNIT(2)—this work; frozen orbital calculation (see Sec. IV B 2),
SC—surface-current model of Sliv [27],
SCF—self-consistent field.

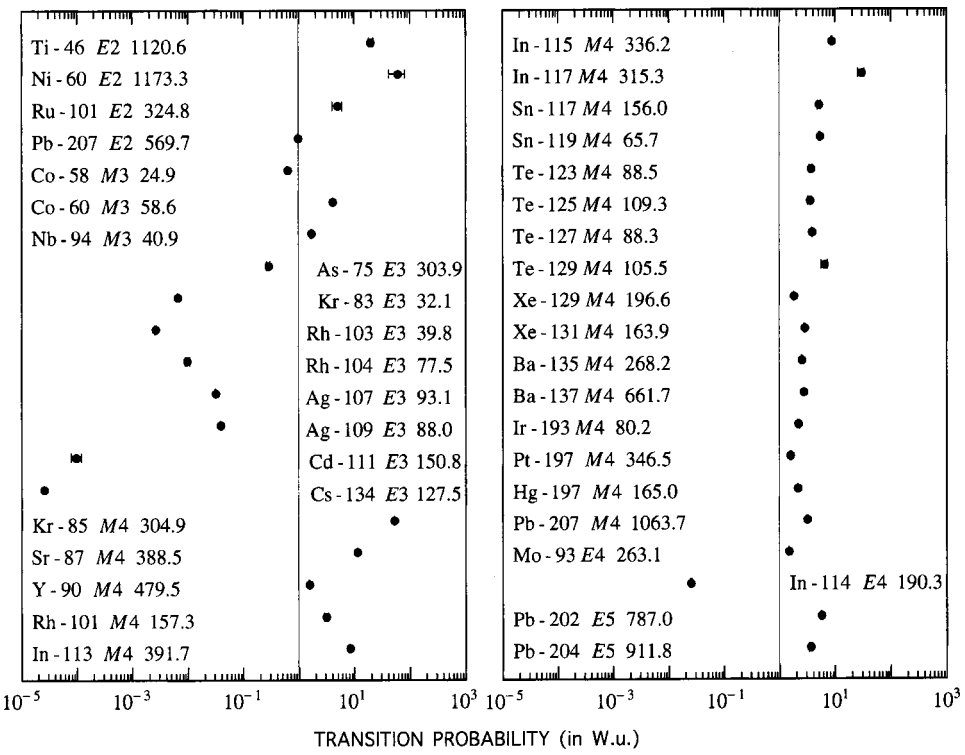

FIG. 2. Strengths of γ-ray transitions classified according to character (E or M, multipolarity).

III. ACCURATE EXPERIMENTAL ICC VALUES

To test the theoretical ICCs, we resort to the philosophy, ''The test of all knowledge is experiment,'' expressed succintly by Feynman *et al.* [28]. We have assembled a database of all ICCs (α_K and α_T) known to better than 5% accuracy. The experimental methods for measuring ICCs have been reviewed by Hamilton [29]. We did not consider dipole transitions because $E1$ transitions are, as a rule, hindered strongly, and $M1$ transitions often appear as mixed $M1+E2$ transitions with uncertain mixing ratios. We evaluated all measurements critically. In a few cases, we have increased the uncertainty values quoted by the authors because we concluded that they had been underestimated. If a particular quantity has been measured more than once, we list the adopted value based on our evaluations. Even though we have examined the unweighted and weighted (inversely proportional to the quoted uncertainty and to the square of the quoted uncertainty) average values, we have not adhered religiously to such procedures in arriving at our adopted values. Moreover, the uncertainty assigned to the adopted value is equal to or larger than the smallest uncertainty assigned to the measured values. In addition, we have listed all measured values (and references) that went into our evaluations.

It is known [30,31] that α_T for a $2_1^+ \rightarrow 0_1^+$, $E2$ transition in an even-even nucleus can be extracted from the $B(E2)\uparrow$ value from Coulomb excitation (with detection of inelasically scattered particles) and the half-life ($T_{1/2}$) value from lifetime measurements. The connecting expression [12] is

$$T_{1/2}(1+\alpha_T) = 2.829 \times 10^{11} E^{-5} [B(E2)\uparrow / e^2 b^2]^{-1}, \quad (1)$$

where the energy of the 2_1^+ state E is in keV, $B(E2)\uparrow$ is in e^2b^2, and τ is in ns. In Table A (see the electronic addendum to this paper [32]), we have used Eq. (1) to extract α_T values for 29 pure $E2$ transitions. All of these α_T values except that for ^{156}Dy (with an uncertainty of 14%) have been carried over to Table B of Ref. [32] where they are supplemented by 21 directly measured ICCs (14 α_K and 7 α_T) bringing the total number of $E2$ cases to 49.

In Table B [32] we have also presented the available data for 51 more cases. The breakdown is as follows: 3 $M3$, 10 $E3$, 34 $M4$, 2 $E4$, and 2 $E5$ transitions. We thus have a total of 100 ICCs (45 α_K and 55 α_T values for 77 transitions), measured with an accuracy of $\leqslant 5\%$, which can be used for testing theory.

The transitions deexciting the states listed in Table A [32] are pure $E2$ because they represent $2_1^+ \rightarrow 0_1^+$ transitions. Radiation with two (rarely three) values of L of the same parity can be present in mixed multipolarity transitions (that is, mixtures of $E2+M3$, $M3+E4$, $E3+M4$, $M4+E5$, etc., are possible) if such transitions are permitted by the selection rules. Based on the scarcity of counterexamples, it is believed that whenever $\Delta J \geqslant 2$ (where ΔJ is the spin difference between the initial and final states) an appreciable part of the γ transition proceeds by the lowest possible multipole order. Higher multipoles occur only when the transition is ''highly'' hindered. We show in Fig. 2 the transition probabilities for those transitions that can be, in principle, mixed. Even though a few transitions (particularly $E3$) appear to be hindered, we initially treat all transitions listed in this work as pure transitions. This is because one of the major arguments used to invoke the presence of a higher-multipolarity component in a particular transition is the departure of the experimental ICC from the theoretical value. Therefore, the overall level of agreement between theory and experiment needs to be examined first and settled. We will return to the hindered transitions in Sec. V.

TABLE I. Underlying assumptions in the calculations leading to various ICC tables.

Hager and Seltzer (HS) [1] Relativistic Hartree-Fock-Slater (RHFS)	Rösel, Fries, Alder, and Pauli (RFAP) [2] Relativistic Hartree-Fock-Slater (RHFS)	Band and Trzhaskovskaya (BT) [3] Relativistic Hartree-Fock-Slater (RHFS)	Band, Trzhaskovskaya, Nestor, Tikkanen, and Raman (BTNTR) [19] Relativistic Dirac-Fock (DF)
A. Atomic Field model			
Self-consistent field calculated in the course of ICC computations. RHFS method with $C=\frac{2}{3}$ in the exchange term.	Used self-consistent potential from Ref. [38]. RHFS method with $C=1$ in the exchange term.	Self-consistent field calculated in the course of ICC computations. RHFS method with $C=1$ in the exchange term.	Self-consistent field calculated in the course of ICC computations. Relativistic DF method with exact treatment of exchange.
B. Consideration of the hole			
Taken into account	Not taken into account	Taken into account	Not taken into account
C. Nuclear model			
Fermi nuclear charge distribution. Dynamic effect not taken into account, NP model.	Potential of a homogeneously charged sphere with a radius $R_0=1.2A^{1/3}$ fm. Dynamic effect not taken into account, NP model.	Potential of a homogeneously charged sphere with a radius $R_0=1.2A^{1/3}$ fm. Dynamic effect taken into account, SC model.	Potential of a homogeneously charged sphere with a radius $R_0=1.2A^{1/3}$ fm. Dynamic effect taken into account, SC model.
D. Experimental elctron binding energies			
Taken from Ref. [34]	Taken from Ref. [34]	Taken from Refs. [35–37]	Taken from Refs. [35–37]
E. Higher-order effects			
Vacuum polarization and electron correlation corrections taken into account approximately	Not taken into account	Not taken into account	Not taken into account
F. Range of atomic numbers			
$30 \le Z \le 103$	$30 \le Z \le 104$	$10 \le Z \le 104$	$10 \le Z \le 126$
G. Atomic shells			
K, L, and M	All shells	K, L, and M	All shells
H. Range of gamma-ray energies (in keV)			
$\varepsilon_i+1 \le E_\gamma \le 1500-1650$ for $i=K$. $\varepsilon_i+1 \le E_\gamma \le 1000-1550$ for $i=L$. $\varepsilon_i+1 \le E_\gamma \le 150-510$ for $i=M$. ICCs for different shells not given for the same set of γ-ray energies for each Z. "Resonance" regions seldom expanded.	$\varepsilon_i+2 \le E_\gamma \le 3000-5000$ for $i=K$. $\varepsilon_i+2 \le E_\gamma \le 1500$ for $i=L$. $\varepsilon_i+2 \le E_\gamma \le 500-1500$ for $i=M$, N, O, P, and Q. ICCs for different shells are given for the same set of -ray energies for each Z. "Resonance" regions often expanded.	$\varepsilon_i+1 \le E_\gamma \le 6000$ for $i=K$. $\varepsilon_i+1 \le E_\gamma \le 2000$ for $i=L$. $\varepsilon_i+1 \le E_\gamma \le 450$ for $i=M$. ICCs for different shells are given for the same set of γ-ray energies for each Z. "Resonance" regions often expanded.	$\varepsilon_i+1 \le E_\gamma \le 2000$ for $i=K$. $\varepsilon_{L_1}+1 \le E_\gamma \le 2000$ for $i=L$. $\varepsilon_{L_1}+1 \le E_\gamma \le 2000$ for $i=M$, N, O, P, Q, and R. ICCs for different shells are given for the same set of γ-ray energies for each Z. "Resonance" regions often expanded.
I. Range of multipolarities			
$1 \le L \le 4$	$1 \le L \le 4$	$1 \le L \le 5$	$1 \le L \le 5$

TABLE II. The quantities $\Delta_{\rm ICC}$ (RHFS:BTNTR) [see Eq. (21)] and $\Delta\rho_i$ (RHFS:BTNTR) [see Eq. (22)] for selected low-multipolarity transitions.

	$^{212}_{83}Bi_{129}$ 238.6-keV, $M1$ transition				$^{166}_{68}Er_{98}$ 80.6-keV, $E2$ transition			
	RHFS1:BTNTR		RHFS$\frac{2}{3}$:BTNTR		RHFS1:BTNTR		RHFS$\frac{2}{3}$:BTNTR	
Shell	$\Delta_{\rm ICC}$	Δ_{ρ_i}	$\Delta_{\rm ICC}$	Δ_{ρ_i}	$\Delta_{\rm ICC}$	Δ_{ρ_i}	$\Delta_{\rm ICC}$	Δ_{ρ_i}
K	1.3	0.4	0.8	–0.1	2.9	0.3	2.0	0.0
L_2	2.6	2.6	0.8	1.0	2.7	2.6	1.0	0.8
L_3	1.4	1.7	0.2	0.2	2.2	2.0	0.6	0.3
M_3	1.5	1.8	–0.2	–0.2	2.2	2.0	–0.2	–0.5
M_4	3.5	4.5	0.5	1.0	4.3	5.1	0.6	0.8
N_1	4.2	3.3	2.5	1.7	6.4	4.4	5.5	3.0
N_2	5.2	5.1	2.7	2.6	6.5	6.5	4.2	4.1
N_6	9.3	10.8	1.1	2.0	15.1	17.0	0.5	1.2
O_1	11.8	11.1	8.9	8.2	18.1	15.9	15.0	12.3
O_3	11.2	11.6	6.8	6.9	18.4	18.2	10.9	10.6
P_1	23.6	23.4	10.2	10.1	50.5	49.3	8.0	6.6

IV. THEORETICAL ICC VALUES

A. Basic formulas for ICC calculations

The relativistic expressions for the ICC $\alpha_i^{\tau L}$ on the ith atomic shell obtained in the framework of the first nonvanishing order of pertubation theory and one-electron approximation is [6,19,33]

$$\alpha_i^{\tau L}=\sum_{\kappa_f}|B_{if}^{\tau L}R_{if}^{\tau L}|^2, \tag{2}$$

where τL is the nuclear transition multipolarity (electric $\tau=E$ or magnetic $\tau=M$) and indices i and f refer, respectively, to the initial (bound) and final (continuum) states of the electron. The relativistic quantum number κ is given by $\kappa=(l-j)(2j+1)$, where j and l are the quantum numbers of the electron total angular momentum and orbital angular momentum, respectively. The summation in Eq. (2) extends over all final states with quantum numbers κ_f that are allowed by the selection rules:

$$|L-j_i|\leq j_f\leq L+j_i, \tag{3a}$$

$$(l_f+l_i+L)\ \text{ is }\ \begin{cases}\text{even for } EL \text{ transitions}\\ \text{odd for } ML \text{ transitions.}\end{cases} \tag{3b}$$

For electric transitions, the angular part $B_{if}^{\tau L}$ and the radial part $R_{if}^{\tau L}$ are given by

$$B_{if}^{EL}=(-1)^{j_f+1/2+L}C_{l_i0l_f0}^{L0}W(l_ij_il_fj_f;\tfrac{1}{2}L)\times\left[\pi k\alpha\frac{(2j_i+1)(2l_i+1)(2j_f+1)(2l_f+1)}{L(L+1)(2L+1)}\right]^{1/2} \tag{4}$$

and

$$R_{if}^{EL}=(\kappa_i-\kappa_f)(R_{1,\Lambda=L-1}+R_{2,\Lambda=L-1})+L(R_{2,\Lambda=L-1}-R_{1,\Lambda=L-1}+R_{3,\Lambda=L}). \tag{5}$$

For magnetic transitions, the corresponding expressions are

$$B_{if}^{ML}=(-1)^{j_f+1/2+L}C_{l_i0\bar{l}_f0}^{L0}W(l_ij_i\bar{l}_fj_f;\tfrac{1}{2}L)\times\left[\pi k\alpha\frac{(2j_i+1)(2l_i+1)(2j_f+1)(2\bar{l}_f+1)}{L(L+1)(2L+1)}\right]^{1/2} \tag{6}$$

and

$$R_{if}^{ML}=(\kappa_i+\kappa_f)(R_{1,\Lambda=L}+R_{2,\Lambda=L}). \tag{7}$$

In Eq. (4), $C_{l_i0l_f0}^{L0}$ is a Clebsch-Gordan coefficient, $W(l_ij_il_fj_f;\frac{1}{2}L)$ is a Racah coefficient, k is the γ-ray energy, and $\alpha=e^2/\hbar c$ is the fine structure constant. In Eq. (6), the symbols $C_{l_i0\bar{l}_f0}^{L0}$, $W(l_ij_i\bar{l}_fj_f;\frac{1}{2}L)$, k, and α have similar meanings; in addition, $\bar{l}=2j-l$. The radial parts, Eqs. (5) and (7), contain three kinds of radial integrals:

$$R_{1,\Lambda}=\int_0^\infty G_iF_fX_\Lambda(kr)dr, \tag{8a}$$

$$R_{2,\Lambda}=\int_0^\infty F_iG_fX_\Lambda(kr)dr, \tag{8b}$$

$$R_{3,\Lambda}=\int_0^\infty (G_iG_f+F_iF_f)X_\Lambda(kr)dr, \tag{8c}$$

where $G(r)=rg(r)$ and $F(r)=rf(r)$. The large and small components of the relativistic radial electron wave function are represented by $g(r)$ and $f(r)$, respectively. In any calculation, if $G_i(F_i)$ and $G_f(F_f)$ are generated in the *same* atomic field, they are orthogonal.

The radial part of the transition potential $X_\Lambda(kr)$ is written in the surface-current (SC) model of Sliv [27] as

TABLE III. The quantities Δ_{ICC} (RFHS1:BTNTR) [see Eq. (21)] and Δ_{ρ_i} (RHFS1:BTNTR) [see Eq. (22)] for high-multipolarity transitions.

	Δ_{ICC} (RHFS1:BTNTR)						$\Delta\rho_i$ (RHFS1:BTNTR)
E_k (keV)	$E3$	$E4$	$E5$	$M3$	$M4$	$M5$	
			Niobium ($Z=41$) K shell				$Z=41$, K shell
50	2.3	2.8	3.2	2.9	3.4	3.9	0.5
100	1.6	1.9	2.1	2.2	2.6	2.9	0.5
200	1.2	1.4	1.6	1.7	2.0	2.2	0.5
300	1.0	1.2	1.3	1.4	1.7	1.9	0.5
			Niobium ($Z=41$) L_1 shell				$Z=41$, L_1 shell
50	2.6	3.3	4.3	3.6	4.0	4.6	0.7
100	1.6	1.8	2.0	2.9	3.2	3.5	0.7
200	1.2	1.4	1.5	1.5	1.8	2.8	0.7
300	1.1	1.3	1.4	1.2	1.5	2.5	0.7
			Niobium ($Z=41$) L_3 shell				$Z=41$, L_3 shell
50	3.9	4.3	4.7	5.0	5.8	6.3	3.1
100	3.6	3.9	4.1	4.5	5.2	5.4	3.1
200	3.4	3.7	3.8	3.5	4.0	4.8	3.1
300	3.3	3.4	3.7	3.6	4.0	4.5	3.1
			Thorium ($Z=90$) K shell				$Z=90$, K shell
50	3.2	4.2	4.9	2.7	4.0	4.7	0.4
100	2.5	3.2	3.7	2.1	3.2	3.6	0.4
200	1.8	2.3	2.7	1.7	2.6	2.8	0.4
300	1.5	1.8	2.0	1.5	1.8	2.1	0.4
			Thorium ($Z=90$) L_1 shell				$Z=90$, L_1 shell
50	3.1	4.0	4.7	3.4	4.1	5.1	0.8
100	2.7	3.2	3.9	2.8	3.3	4.1	0.8
200	2.5	2.7	3.3	2.3	2.7	3.3	0.8
300	2.2	2.5	2.9	2.2	2.4	3.0	0.8

$$X_\Lambda(kr)=\begin{cases} j_\Lambda(kr)\dfrac{h_\Lambda(kR_0)}{j_\Lambda(kR_0)} & \text{for } r\leqslant R_0 \\ h_\Lambda(kr) & \text{for } r>R_0, \end{cases} \tag{9}$$

and in the no-penetration (NP) model of Rose [6] as

$$X_\Lambda(kr)=h_\Lambda(kr). \tag{10}$$

The spherical Bessel and Hankel functions are defined by

$$j_\nu(x)=\sqrt{\frac{\pi}{2x}}J_{\nu+1/2}(x) \quad \text{and} \quad h_\nu(x)=\sqrt{\frac{\pi}{2x}}\mathcal{H}^{(1)}_{\nu+1/2}(x), \tag{11}$$

where $J_{\nu+1/2}$ is a Bessel function and $\mathcal{H}^{(1)}_{\nu+1/2}(x)$ is a Hankel function of the first kind. All expressions make use of relativistic units where the electron Compton wavelength ($\hbar/m_0c$) serves as a unit of length and the electron rest mass (m_0c^2) as a unit of energy. In calculating the continuum wave functions, the conversion electron energy E_k is determined by

$$E_k=E_\gamma-\varepsilon_i, \tag{12}$$

where E_γ is the γ-ray energy ($k=E_\gamma$ in relativistic units) and ε_i is the binding energy for the ith atomic shell. The binding energies are taken from experiment [34–37] if available.

The electron wave functions $G(r)$ and $F(r)$ are solutions of the system of Dirac equations

$$\frac{dG}{dr}=-\frac{\kappa}{r}G+[E+1-V(r)]F, \tag{13a}$$

$$\frac{dF}{dr}=+\frac{\kappa}{r}F-[E-1-V(r)]G, \tag{13b}$$

where E is the total electron energy including the electron rest mass ($E<1$ for the bound electron state and $E>1$ for the continuum state) and $V(r)$ is the potential energy of an electron in the field of a nucleus and other atomic electrons. The potential $V(r)$ consists of three parts: (i) $V_{\mathrm{nucl}}(r)$, the interaction of the electron with the nucleus, (ii) $V_{\mathrm{coul}}(r)$, the

TABLE IV. The quantities Δ_{ICC} (RHFS:BTNTR) [see Eq. (21)] and Δ_{ρ_i} (RHFS:BTNTR) [see Eq. (22)] for very low-energy transitions and outer shells in selected nuclei.

				RHFS1:BTNTR		RHFS$\frac{2}{3}$:BTNTR	
Nucleus	E_γ(keV)	τL	Shell	Δ_{ICC}	Δ_{ρ_i}	Δ_{ICC}	Δ_{ρ_i}
$^{110}_{47}Ag_{63}$	1.280	$M3$	M_1	12	1	6	0
			M_2	23	4	13	0
			M_3	11	3	6	0
			M_5	14	8	6	0
			N_2	31	15	23	11
			O_1	59	46	12	7
$^{183}_{74}W_{109}$	0.545	$E1$	N_2	–13	5	0	3
			N_3	–62	4	–47	1
			N_4	273	7	209	2
			N_5	166	7	131	2
			O_1	–34	14	–30	10
			O_2	–41	19	–39	12
			O_3	–15	14	13	7
			O_4	144	24	102	–1
			P_1	–19	38	–33	9
$^{235}_{92}U_{143}$	0.075	$E3$	P_2	28	14	17	7
			P_3	39	16	30	7
			P_4	46	23	–1	–18
			O_6	50	27	23	2
			Q_1	68	36	23	3

TABLE V. The quantity Δ_{ρ_κ} (RHFS:BTNTR) [see Eq. (23)] for the free electron corresponding to different values of the relativistic quantum number κ.

	$E_k = 0.1$ keV		$E_k = 0.5$ keV		$E_k = 5.0$ keV		$E_k = 50.0$ keV	
	Δ_{ρ_κ} (RHFS:BTNTR)		Δ_{ρ_κ} (RHFS:BTNTR)		Δ_{ρ_κ} (RHFS:BTNTR)		Δ_{ρ_κ} (RHFS:BTNTR)	
κ	RHFS1	RHFS$\frac{2}{3}$	RHFS1	RHFS$\frac{2}{3}$	RHFS1	RHFS$\frac{2}{3}$	RHFS1	RHFS$\frac{2}{3}$
				Niobium ($Z = 41$)				
–1	7.3	7.4	3.6	3.6	1.1	1.1	0.4	0.3
+1	8.9	8.5	4.3	3.6	1.7	1.1	0.8	0.5
+2	13	11	5.5	3.3	3.2	2.1	1.3	0.9
+3	35	23	13	8.1	4.7	3.2	1.5	1.1
+4	71	56	22	16	5.9	4.3	1.7	1.2
+5	79	65	25	20	6.7	5.1	1.9	1.4
				Thorium ($Z = 90$)				
–1	7.0	6.9	3.3	3.2	1.4	1.2	0.6	0.5
+1	8.4	7.9	4.1	3.7	1.9	1.4	1.1	0.7
+2	10	9.4	5.3	4.2	2.2	1.2	1.5	1.0
+3	10	8.0	6.2	3.8	3.8	2.3	1.9	1.3
+4	68	45	14	7.6	5.6	3.6	2.3	1.6
+5	89	64	27	18	7.3	5.2	2.5	1.8

TABLE VI. The quantity Δ_{ICC} (hole : no hole) [see Eq. (21)] calculated with and without the hole resulting from the ejection of the conversion electron. The calculations were performed by the DF method for $Z=92$.

E_k (keV)	$M1$	$E2$	$M3$	$E4$	$E5$	$M1$	$E2$	$M3$	$E4$	$E5$
			K shell					L_1 shell		
0.05	0.0	7.7	8.3	208	173	0.0	3.5	5.4	211	174
0.5	0.4	5.2	5.9	18	22	0.2	1.2	3.1	17	22
1.0	0.4	5.3	5.9	13	15	0.2	1.3	3.1	12	15
10.0	0.5	4.2	4.8	6.1	6.0	0.2	0.6	2.3	4.6	5.0
100.0	0.4	1.9	2.5	2.6	2.8	0.1	0.6	0.8	1.2	1.5
200.0	0.2	1.2	1.9	2.0	2.1	0.0	0.5	0.6	0.7	0.9
500.0	0.1	0.5	1.2	1.3	1.5	0.0	0.2	0.3	0.4	0.6
			L_2 shell					M_1 shell		
0.05	1.2	2.5	9.3	7.7	214	0.0	3.9	3.1	221	174
0.5	0.4	0.2	8.4	8.7	17	0.3	1.4	0.9	16	21
1.0	0.4	0.2	7.7	7.9	13	0.2	1.5	1.0	11	13
10.0	0.4	0.1	4.2	4.4	5.2	0.1	0.6	0.7	3.5	4.4
100.0	0.1	0.1	1.2	1.3	1.6	0.0	0.1	0.3	0.5	0.6
200.0	0.1	0.1	0.7	0.8	1.0	0.0	0.1	0.2	0.3	0.4
500.0	0.0	0.0	0.3	0.4	0.5	0.0	0.1	0.1	0.1	0.2

Coulomb interaction between all electrons, and (iii) $V_{ex}(r)$, the electron exchange interaction. That is,

$$V(r)=V_{nucl}(r)+V_{coul}(r)+V_{ex}(r). \tag{14}$$

Inside the nucleus, the potential of a homogeneously charged sphere with radius $R_0=1.2A^{1/3}$ fm (A is the mass number) is usually assumed. The nuclear part of the potential has the form

$$V_{nucl}(r)=\begin{cases} -(\alpha Z/2R_0)[3-(r/R_0)^2] & \text{for } r\leqslant R_0 \\ -\alpha Z/r & \text{for } r>R_0. \end{cases} \tag{15}$$

The Coulomb part of the potential may be written as

$$V_{coul}(r)=\frac{\alpha}{r}\sum_A Q_A\left[\int_0^r (G_A^2+F_A^2)dr + r\int_r^\infty \frac{1}{r}(G_A^2+F_A^2)dr\right], \tag{16}$$

where the index A denotes the set of quantum numbers nlj (n is the principal quantum number) and Q_A is the occupation number for an atomic shell. In the RHFS method, the exchange interaction between atomic electrons is taken into account *approximately* on the basis of the statistical model for a free electron gas. In this approximation,

$$V_{ex}(r)=-C\tfrac{3}{2}\alpha\left[\frac{3}{\pi}\rho(r)\right]^{1/3}, \tag{17}$$

where $\rho(r)$ is the spherical-averaged total radial electron density, which is defined as

$$\rho(r)=\sum_A Q_A\frac{G_A^2(r)+F_A^2(r)}{4\pi r^2}. \tag{18}$$

The constant C is discussed in Sec. IV B 1. The DF method treats exchange *exactly*. As a consequence, the expressions for the exchange terms turn out to be more complicated (see Eq. (40) of Ref. [19]) than Eq. (17). The self-interaction of an electron is eliminated from the DF equations whereas it is allowed to remain in the RHFS method.

The wave functions $G(r)$ and $F(r)$ are bounded at origin and at infinity. The bound wave function is normalized so that

$$\int_0^\infty (G^2+F^2)dr=1. \tag{19}$$

TABLE VII. Comparison of experimental ICC values for selected $M4$ transitions with theoretical values calculated within the NP and SC models using the DF method with a hole [RNIT(1)].

			Calculations		
Nucleus	E_γ(keV)	ICC	NP	SC	Exp.
$^{117}_{50}Sn_{67}$	156.0	α_T	47.08	46.80	46.40±0.25
$^{137}_{56}Ba_{81}$	661.6	α_K	0.0922	0.0914	0.0902±0.0008
$^{197}_{80}Hg_{117}$	165.0	α_K	75.29	73.79	73.9±0.08
$^{207}_{82}Pb_{125}$	1063.7	α_K	0.0964	0.0942	0.0945±0.0022

TABLE VIII. Comparison between experimental and theoretical internal conversion coefficients.

Nucleus	Transition Energy[a] (keV)	Multi-polarity	Experiment Meas-ured	Experiment Value[a,b]	Theoretical conversion coefficients[c] Ref. [1] RHFS HS	Ref. [2] RHFS RFAP	Ref. [3] RHFS BT	Ref. [19] DF BTNTR	This work[d] DF RNIT(1)	This work[d] DF RNIT(2)
$^{46}_{22}Ti_{24}$	889.286 *3*	*E2*	α_T	0.000160 *7*			0.0001639	0.0001626	0.0001625	0.0001625
$^{46}_{22}Ti_{24}$	1120.560 *4*	*E2*	α_T	0.000095 *4*			0.0000932	0.0000925	0.0000924	0.0000924
$^{54}_{24}Cr_{30}$	834.855 *3*	*E2*	α_K	0.000224 *10*			0.0002233	0.0002220	0.0002218	0.0002218
$^{54}_{24}Cr_{30}$	834.855 *3*	*E2*	α_T	0.000251 *11*			0.0002472	0.0002453	0.0002452	0.0002452
$^{58}_{26}Fe_{32}$	810.764 *15*	*E2*	α_K	0.00030 *1*			0.0003012	0.0002996	0.0002995	0.0002994
$^{58}_{26}Fe_{32}$	810.764 *15*	*E2*	α_T	0.00034 *1*			0.0003346	0.0003324	0.0003322	0.0003322
$^{60}_{28}Ni_{32}$	1173.251 *4*	*E2*	α_K	0.000150 *6*			0.0001508	0.0001502	0.0001500	0.0001500
$^{60}_{28}Ni_{32}$	1173.251 *4*	*E2*	α_T	0.000168 *7*			0.0001679	0.0001670	0.0001669	0.0001668
$^{60}_{28}Ni_{32}$	1332.516 *5*	*E2*	α_K	0.000115 *6*			0.0001142	0.0001138	0.0001137	0.0001137
$^{60}_{28}Ni_{32}$	1332.516 *5*	*E2*	α_T	0.000128 *4*			0.0001271	0.0001266	0.0001265	0.0001264
$^{101}_{44}Ru_{57}$	324.8 *2*	*E2*	α_K	0.0160 *8*	0.01781	0.0179	0.01786	0.01761	0.01767	0.01768
$^{150}_{60}Nd_{90}$	130.21 *8*	*E2*	α_T	0.83 *5*	0.8655	0.863	0.8710	0.8469	0.8555	0.8570
$^{152}_{62}Sm_{90}$	121.782 *1*	*E2*	α_K	0.669 *8*	0.6848	0.676	0.6862	0.6646	0.6761	0.6781
$^{152}_{62}Sm_{90}$	121.782 *1*	*E2*	α_T	1.14 *2*	1.167	1.17	1.175	1.141	1.152	1.155
$^{154}_{62}Sm_{92}$	81.976 *18*	*E2*	α_T	4.83 *11*	4.931	4.93	4.978	4.803	4.856	4.865
$^{152}_{64}Gd_{88}$	344.282 *2*	*E2*	α_K	0.0286 *8*	0.03111	0.0311	0.03123	0.03081	0.03100	0.03102
$^{154}_{64}Gd_{90}$	123.071 *2*	*E2*	α_K	0.634 *16*	0.6623	0.653	0.6637	0.6421	0.6536	0.6557
$^{154}_{64}Gd_{90}$	123.071 *2*	*E2*	α_T	1.20 *2*	1.200	1.20	1.209	1.173	1.185	1.187
$^{156}_{64}Gd_{92}$	88.967 *2*	*E2*	α_T	4.09 *13*	3.933	3.92	3.967	3.831	3.870	3.878
$^{158}_{64}Gd_{94}$	79.510 *2*	*E2*	α_T	6.04 *18*	6.019	6.00	6.078	5.861	5.921	5.932
$^{160}_{64}Gd_{96}$	75.26 *1*	*E2*	α_T	7.41 *21*	7.435	7.42	7.513	7.242	7.314	7.328
$^{158}_{66}Dy_{92}$	98.918 *2*	*E2*	α_T	2.81 *18*	2.859	2.85	2.887	2.791	2.819	2.824
$^{160}_{66}Dy_{94}$	86.788 *1*	*E2*	α_K	1.53 *6*	1.585	1.55	1.592	1.513	1.556	1.565
$^{160}_{66}Dy_{94}$	86.788 *1*	*E2*	α_T	4.61 *11*	4.686	4.68	4.737	4.574	4.618	4.627
$^{162}_{66}Dy_{96}$	80.660 *2*	*E2*	α_T	6.03 *14*	6.219	6.21	6.288	6.067	6.123	6.136
$^{164}_{66}Dy_{98}$	73.392 *5*	*E2*	α_T	8.92 *19*	9.020	9.01	9.121	8.798	8.873	8.891
$^{164}_{68}Er_{96}$	91.40 *2*	*E2*	α_T	4.32 *21*	4.198	4.21	4.242	4.099	4.136	4.144
$^{166}_{68}Er_{98}$	80.577 *7*	*E2*	α_K	1.67 *5*	1.706	1.65	1.704	1.606	1.659	1.671
$^{166}_{68}Er_{98}$	80.577 *7*	*E2*	α_T	6.77 *14*	6.881	6.90	6.95	6.713	6.768	6.780
$^{168}_{68}Er_{100}$	79.804 *1*	*E2*	α_T	7.02 *19*	7.143	7.16	7.222	6.975	7.032	7.044
$^{170}_{68}Er_{102}$	78.591 *22*	*E2*	α_T	7.55 *20*	7.592	7.62	7.677	7.414	7.474	7.487
$^{170}_{70}Yb_{100}$	84.255 *1*	*E2*	α_K	1.40 *4*	1.437	1.39	1.434	1.352	1.396	1.406
$^{172}_{70}Yb_{102}$	78.743 *1*	*E2*	α_T	8.39 *25*	8.365	8.41	8.465	8.183	8.241	8.253
$^{174}_{70}Yb_{104}$	76.471 *1*	*E2*	α_T	9.08 *35*	9.425	9.48	9.543	9.225	9.289	9.303
$^{176}_{70}Yb_{106}$	82.13 *2*	*E2*	α_T	6.95 *26*	7.058	7.08	7.135	6.898	6.949	6.959

TABLE VIII. (*Continued.*)

	Transition		Experiment		Theoretical conversion coefficients[c]					
					Ref. [1]	Ref. [2]	Ref. [3]	Ref. [19]	This work[d]	
Nucleus	Energy[a] (keV)	Multi-polarity	Meas-ured	Value[a,b]	RHFS HS	RHFS RFAP	RHFS BT	DF BTNTR	DF RNIT(1)	DF RNIT(2)
$^{178}_{72}Hf_{106}$	93.180 *1*	*E2*	α_T	4.56 *13*	4.736	4.74	4.775	4.620	4.654	4.661
$^{180}_{72}Hf_{108}$	93.326 *2*	*E2*	α_T	4.48 *6*	4.707	4.71	4.746	4.591	4.625	4.632
$^{182}_{74}W_{108}$	100.106 *1*	*E2*	α_T	3.76 *10*	3.953	3.96	3.984	3.856	3.883	3.889
$^{184}_{74}W_{110}$	111.208 *4*	*E2*	α_T	2.45 *8*	2.610	2.61	2.631	2.548	2.567	2.571
$^{186}_{74}W_{112}$	122.33 *7*	*E2*	α_T	1.68 *11*	1.810	1.81	1.824	1.767	1.781	1.784
$^{198}_{80}Hg_{118}$	411.805 *2*	*E2*	α_K	0.0298 *3*	0.03014	0.0302	0.03017	0.02974	0.02995	0.02997
$^{200}_{80}Hg_{120}$	367.944 *10*	*E2*	α_K	0.0397 *8*	0.03913	0.0391	0.03912	0.03848	0.03880	0.03883
$^{207}_{82}Pb_{125}$	569.703 *2*	*E2*	α_K	0.0157 *5*	0.01590	0.0160	0.01592	0.01575	0.01582	0.01583
$^{230}_{90}Th_{140}$	53.20 *2*	*E2*	α_T	229 *7*	233	233	234.2	227.6	227.8	227.9
$^{232}_{90}Th_{142}$	49.369 *9*	*E2*	α_T	303 *14*	334	335	336.5	326.9	327.2	327.3
$^{234}_{92}U_{142}$	43.498 *1*	*E2*	α_T	660 *19*	727	731	733.4	711.9	712.7	712.9
$^{236}_{92}U_{144}$	45.242 *3*	*E2*	α_T	548 *16*	602	604	605.6	588.0	588.6	588.8
$^{238}_{94}Pu_{144}$	44.08 *3*	*E2*	α_T	756 *22*	803	807	810.0	785.7	786.7	786.9
$^{240}_{94}Pu_{146}$	42.824 *8*	*E2*	α_T	904 *30*	925	928	932.3	904.0	905.2	905.5
$^{58}_{27}Co_{31}$	24.889 *21*	*M3*	α_K	2030 *90*			1894	1753	1821	1839
$^{60}_{27}Co_{33}$	58.59 *1*	*M3*	α_K	41.2 *18*			40.16	38.41	39.18	39.33
$^{94}_{41}Nb_{53}$	40.902 *12*	*M3*	α_K	750 *37*	783.8	781	786.5	730.7	758.7	765.8
$^{75}_{33}As_{42}$	303.925 *2*	*E3*	α_K	0.0472 *23*	0.04701	0.0471	0.04730	0.04663	0.04689	0.04694
$^{83}_{36}Kr_{47}$	32.147 *2*	*E3*	α_K	454 *15*	495.9	477	494.9	458.1	477.1	483.1
$^{103}_{45}Rh_{58}$	39.756 *6*	*E3*	α_K	136 *6*	139.4	133	138.8	127.3	133.1	135.1
$^{103}_{45}Rh_{58}$	39.756 *6*	*E3*	α_T	1510 *30*	1462	1450	1459	1387	1398	1402
$^{104}_{45}Rh_{59}$	77.548 *2*	*E3*	α_T	39 *1*	44.19	44.3	44.80	42.95	43.43	43.57
$^{107}_{47}Ag_{60}$	93.13 *2*	*E3*	α_K	9.2 *4*	9.391	9.23	9.397	9.034	9.227	9.273
$^{109}_{47}Ag_{62}$	88.034 *2*	*E3*	α_K	11.3 *3*	11.56	11.3	11.57	11.10	11.35	11.41
$^{109}_{47}Ag_{62}$	88.034 *2*	*E3*	α_T	25.4 *5*	26.68	26.8	27.04	25.97	26.25	26.33
$^{111}_{48}Cd_{63}$	150.824 *17*	*E3*	α_T	2.12 *11*	2.301	2.31	2.326	2.256	2.278	2.283
$^{134}_{55}Cs_{79}$	127.502 *3*	*E3*	α_K	2.60 *4*	2.771	2.73	2.775	2.677	2.730	2.741
$^{85}_{36}Kr_{49}$	304.871 *20*	*M4*	α_K	0.432 *20*	0.4365	0.438	0.4390	0.4293	0.4331	0.4337
$^{85}_{36}Kr_{49}$	304.871 *20*	*M4*	α_T	0.509 *24*	0.5244	0.518	0.5191	0.5068	0.5108	0.5114
$^{87}_{38}Sr_{49}$	388.532 *3*	*M4*	α_K	0.175 *6*	0.1824	0.183	0.1833	0.1796	0.1810	0.1813
$^{87}_{38}Sr_{49}$	388.532 *3*	*M4*	α_T	0.212 *2*	0.2178	0.216	0.2160	0.2113	0.2128	0.2130
$^{90}_{39}Y_{51}$	479.50 *5*	*M4*	α_K	0.0856 *29*	0.08288	0.0834	0.08335	0.08186	0.08240	0.08249
$^{90}_{39}Y_{51}$	479.50 *5*	*M4*	α_T	0.100 *4*	0.09835	0.0976	0.09763	0.09573	0.09629	0.09639
$^{101}_{45}Rh_{56}$	157.32 *4*	*M4*	α_K	21.2 *10*	21.38	21.3	21.51	20.67	21.05	21.13
$^{113}_{49}In_{64}$	391.691 *8*	*M4*	α_K	0.438 *7*	0.4484	0.449	0.4505	0.4384	0.4430	0.4437

TABLE VIII. (*Continued.*)

Nucleus	Transition Energy[a] (keV)	Multi-polarity	Meas-ured	Experiment Value[a,b]	Theoretical conversion coefficients[c] Ref. [1] RHFS HS	Ref. [2] RHFS RFAP	Ref. [3] RHFS BT	Ref. [19] DF BTNTR	This work[d] DF RNIT(1)	DF RNIT(2)
$^{113}_{49}In_{64}$	391.691 *8*	*M*4	α_T	0.540 *6*	0.5568	0.559	0.5600	0.5452	0.5499	0.5507
$^{115}_{49}In_{66}$	336.24 *3*	*M*4	α_K	0.843 *12*	0.8659	0.865	0.8698	0.8445	0.8544	0.8560
$^{115}_{49}In_{66}$	336.24 *3*	*M*4	α_T	1.073 *14*	1.094	1.10	1.100	1.068	1.079	1.081
$^{117}_{49}In_{68}$	315.302 *12*	*M*4	α_T	1.414 *25*	1.464	1.47	1.471	1.428	1.442	1.444
$^{117}_{50}Sn_{67}$	156.02 *3*	*M*4	α_K	30.2 *15*	31.63	31.4	31.78	30.40	31.01	31.12
$^{117}_{50}Sn_{67}$	156.02 *3*	*M*4	α_T	46.40 *25*	47.79	47.8	48.10	46.14	46.80	46.94
$^{119}_{50}Sn_{69}$	65.66 *1*	*M*4	α_K	1700 *80*	1661	1620	1668	1543	1602	1618
$^{123}_{52}Te_{71}$	88.46 *3*	*M*4	α_T	1050 *40*	1152	1150	1159	1099	1116	1121
$^{125}_{52}Te_{73}$	109.276 *15*	*M*4	α_K	167 *7*	188.6	186	189.7	179.4	184.1	185.1
$^{125}_{52}Te_{73}$	109.276 *15*	*M*4	α_T	355 *11*	363.6	364	366.1	348.5	354.0	355.4
$^{127}_{52}Te_{75}$	88.26 *8*	*M*4	α_K	484 *23*	497.2	487	498.9	467.6	482.0	485.3
$^{129}_{52}Te_{77}$	105.50 *5*	*M*4	α_K	213 *10*	221.8	219	223.0	210.5	216.2	217.4
$^{129}_{54}Xe_{75}$	196.56 *3*	*M*4	α_K	13.61 *67*	13.92	13.8	13.94	13.37	13.61	13.66
$^{131}_{54}Xe_{77}$	163.931 *8*	*M*4	α_K	31.3 *10*	32.13	31.9	32.28	30.81	31.45	31.57
$^{135}_{56}Ba_{79}$	268.219 *20*	*M*4	α_K	3.88 *13*	3.848	3.84	3.867	3.726	3.784	3.793
$^{135}_{56}Ba_{79}$	268.219 *20*	*M*4	α_T	5.42 *11*	5.395	5.41	5.427	5.234	5.296	5.307
$^{137}_{56}Ba_{81}$	661.660 *3*	*M*4	α_K	0.0902 *8*	0.09261	0.0929	0.09289	0.09067	0.09138	0.09148
$^{137}_{56}Ba_{81}$	661.660 *3*	*M*4	α_T	0.1108 *7*	0.1148	0.114	0.1143	0.1115	0.1123	0.1124
$^{193}_{77}Ir_{116}$	80.22 *2*	*M*4	α_K	104 *3*	110.3	103	107.9	91.93	99.47	103.2
$^{193}_{77}Ir_{116}$	80.22 *2*	*M*4	α_T	21300 *700*	22020	22200	22050	20920	21070	21150
$^{197}_{78}Pt_{119}$	346.5 *2*	*M*4	α_K	4.02 *8*	4.401	4.38	4.344	4.187	4.261	4.272
$^{197}_{78}Pt_{119}$	346.5 *2*	*M*4	α_T	7.7 *4*	7.714	7.74	7.643	7.385	7.468	7.483
$^{197}_{80}Hg_{117}$	164.97 *7*	*M*4	α_K	73.9 *8*	77.05	76.0	76.08	71.69	73.79	74.26
$^{197}_{80}Hg_{117}$	164.97 *7*	*M*4	α_T	340 *5*	348.1	350	347.1	331.4	334.8	335.8
$^{207}_{82}Pb_{125}$	1063.662 *4*	*M*4	α_K	0.0945 *22*	0.09695	0.0977	0.09491	0.09338	0.09417	0.09427
$^{207}_{82}Pb_{125}$	1063.662 *4*	*M*4	α_T	0.126 *3*	0.1295	0.130	0.1271	0.1248	0.1256	0.1257
$^{93}_{42}Mo_{51}$	263.062 *5*	*E*4	α_T	0.690 *17*	0.7193	0.704	0.7084	0.6905	0.6962	0.6976
$^{114}_{49}In_{65}$	190.29 *3*	*E*4	α_K	2.50 *5*	2.584	2.55	2.589	2.514	2.553	2.561
$^{202}_{82}Pb_{120}$	786.99 *6*	*E*5	α_K	0.088 *4*			0.08263	0.08064	0.08155	0.08167
$^{204}_{82}Pb_{122}$	911.78 *7*	*E*5	α_K	0.0548 *20*			0.05501	0.05378	0.05432	0.05439

[a]According to our notation, 889.286 *3* ≡ 889.286 ± 0.003, 0.000160 *7* ≡ 0.000160 ± 0.000007, etc.

[b]Adopted ICC values from Table B of Ref. [32].

[c]See also Table I.

[d]The hole after conversion is taken into account in the current work. To obtain the RNIT(1) results, the continuum wave functions were computed in the SCF potential for the positive ion. To obtain the RNIT(2) results, the continuum wave functions were computed in the "frozen orbital" approximation.

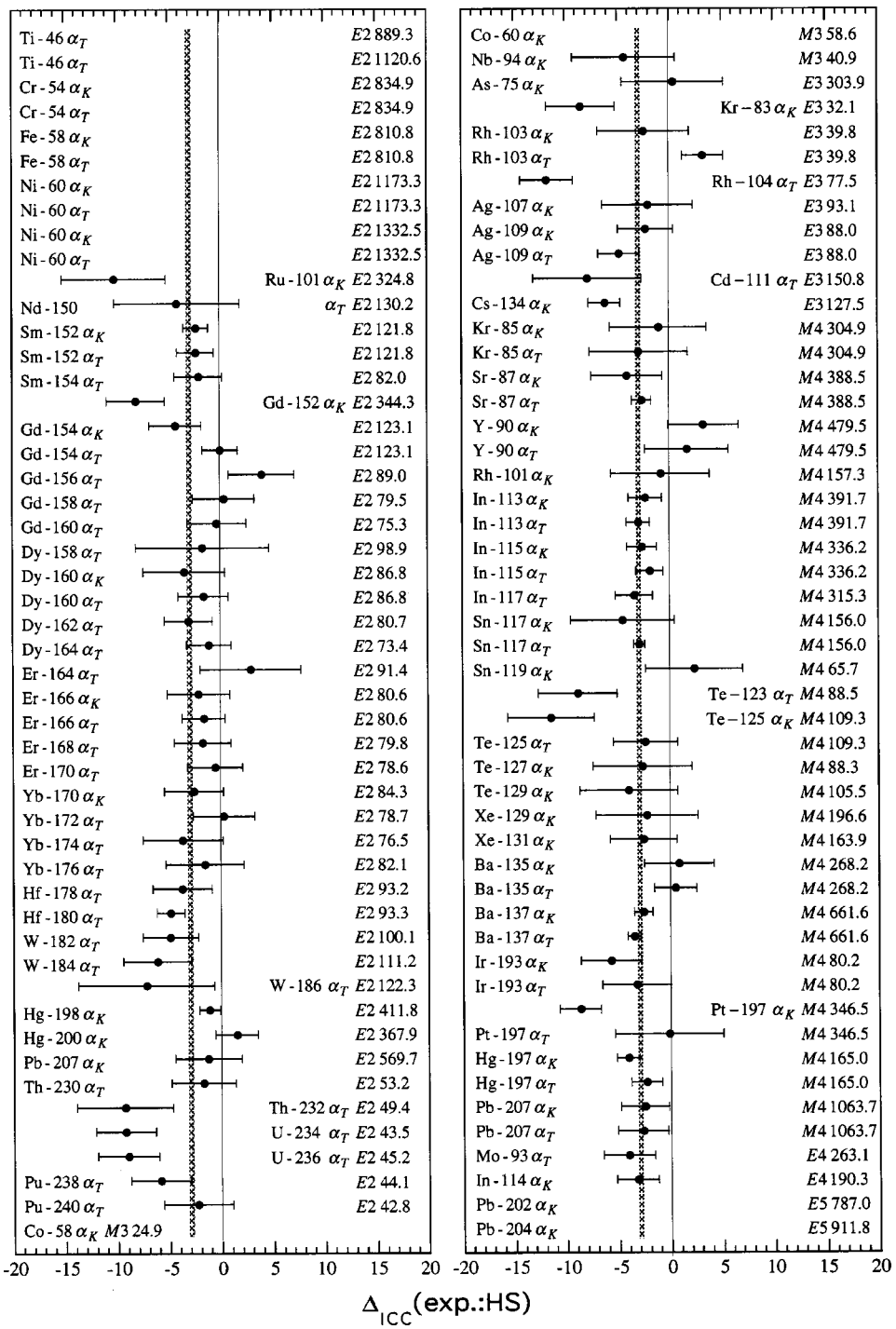

FIG. 3. Comparison between measured conversion coefficients and theoretical Hager and Seltzer (HS) values. See Eq. (21) for the definition of Δ_{ICC}. The data points and error bars are based on the values given in Table VIII. The average difference is $(-3.01 \pm 0.24)\%$ for these 86 data points.

The continuum wave function is normalized per unit energy range to give

$$\lim_{r\to\infty}\left[G^2+\frac{E+1}{E-1}F^2\right]=\frac{1}{\pi}\sqrt{\frac{E+1}{E-1}}. \tag{20}$$

Sections 3.1 and 3.2 of Ref. [19] describe how the wave functions are computed numerically in the DF method (see especially Fig. 1 of Ref. [19]). Similar techniques are employed in the computations by the RHFS method. The Hankel and Bessel functions involved in the computation can be obtained through well-known recursion relations. Substituting the wave functions and the radial part of the transition potential into Eq. (8), one may calculate the radial integrals, and finally the ICC.

B. Comparison of various ICC calculations

To understand the differences in the theoretical ICC values, we need to examine more closely the physical assumptions underlying different widely used calculations. We list first the assumptions that are common to all calculations.

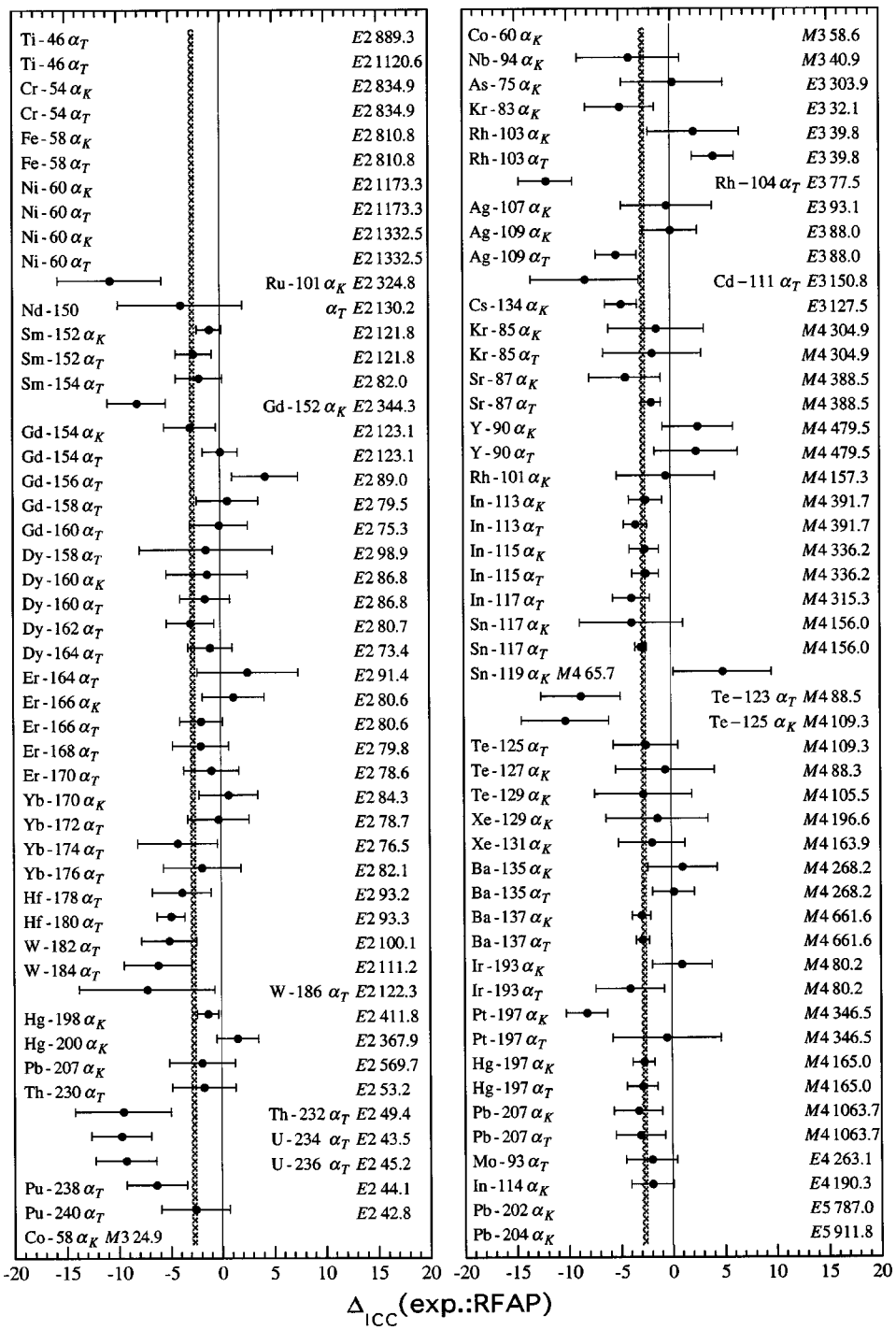

FIG. 4. Comparison between measured conversion coefficients and theoretical Rösel, Fries, Alder, and Pauli (RFAP) values. See Eq. (21) for the definition of Δ_{ICC}. The data points and error bars are based on the values given in Table VIII. The average difference is $(-2.71\pm0.24)\%$ for these 86 data points.

They have been carried out (i) in the first nonvanishing order of the perturbation theory, (ii) using the one-electron approximation, (iii) for a free neutral atom, (iv) taking into account the screening of an electric field of a nucleus by atomic electrons, (v) for a spherically symmetric atomic potential, (vi) using relativistic electron wave functions, (vii) taking into consideration the static effect of the nuclear finite size, (viii) for a sperically symmetric nucleus, and (ix) using experimental values of the electron binding energy ε_i in Eq. (12) if available. We then present Table I, which summarizes differences in the underlying assumptions. For instance, RFAP take the self-consistent atomic potential from Ref. [38] whereas HS, BT, and BTNTR calculate a relevant potential in the course of ICC computations. In addition, we give in Table I the atomic number Z, atomic shell, γ-ray energy E_γ, and multipolarity L ranges covered by the listed tables. The tabulated values are for a particular combination of Z (stated) and A (usually unstated) values. The theoretical ICCs are usually obtained by spline interpolation of the tabulated values except in those rare cases when the user has access to the original code used to generate the table.

The HS table gives ICCs only for the K, L, and M shells. The higher N, O, P, Q, and R shells become occupied when the atomic number Z exceeds 18, 36, 54, 86, and 118, respec-

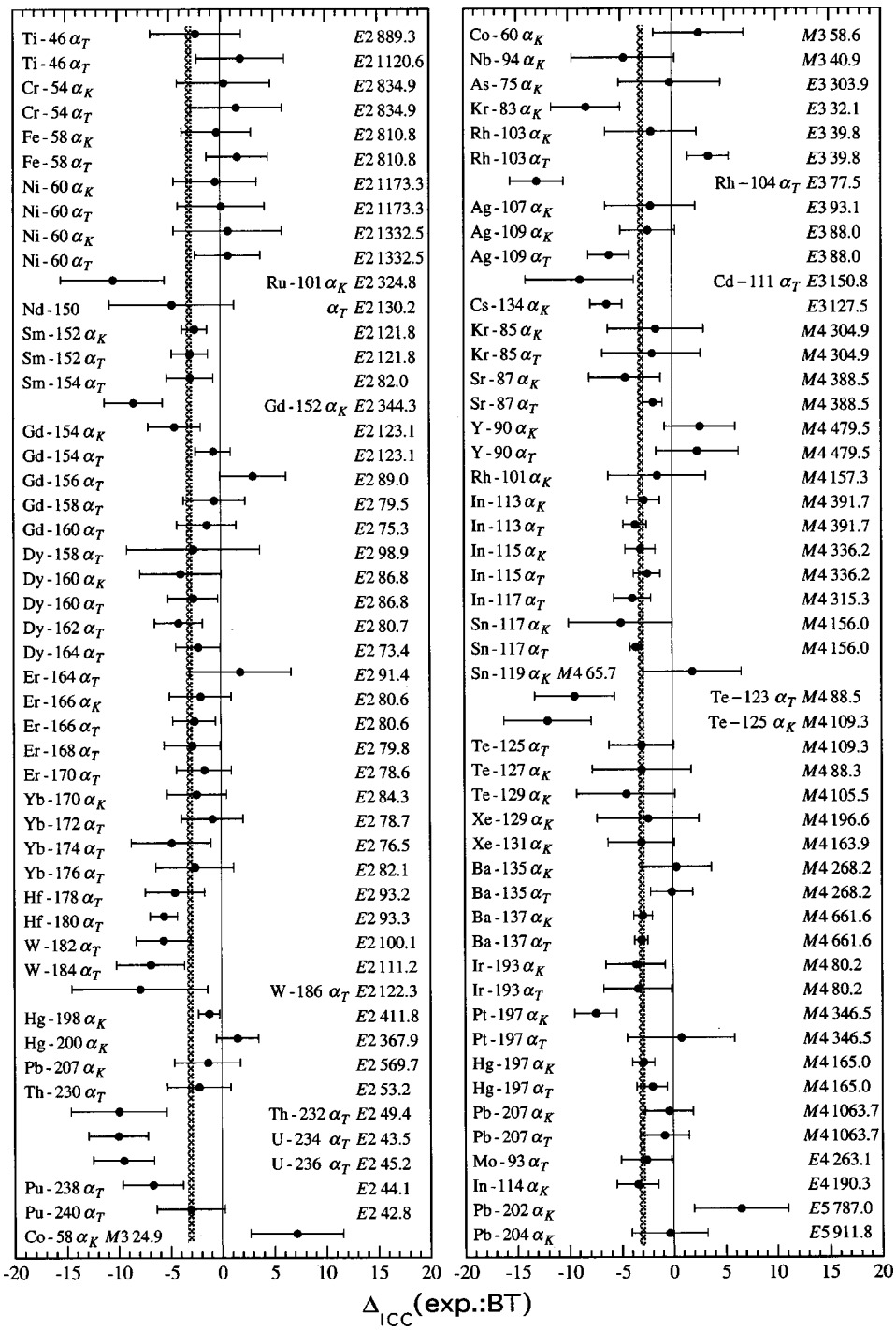

FIG. 5. Comparison between measured conversion coefficients and theoretical Band and Trzhaskovskaya (BT) values. See Eq. (21) for the definition of Δ_{ICC}. The data points and error bars are based on the values given in Table VIII. The average difference is $(-3.04\pm0.24)\%$ for these 100 data points.

tively. To obtain α_T for transitions in $30\leqslant Z\leqslant 103$ nuclei, it is customary to supplement the HS values with the values given by Dragoun *et al.* [39,40] for outer-shell contributions. This procedure is followed, for instance, by the evaluators who prepare the *Nuclear Data Sheets*. The RFAP table gives not only the ICCs for all relevant shells but also the α_T values at selected energies. The published BT table is similar to the HS table, in that ICCs are given only for the *K*, *L*, and *M* shells. In this case, we have access to the original code. The BT values given in this paper are those calculated with this code and not derived from the spline interpolation of the values given in Ref. [3]. The DF values are also generated with a code for the actual energy of the γ-ray transition and actual mass number.

In this paper we use Δ_{ICC} to denote the differences between ICCs. We define

$$\Delta_{ICC}(\text{set1}:\text{set2})=\frac{\alpha_i(\text{set1})-\alpha_i(\text{set2})}{\alpha_i(\text{set2})}\times 100. \qquad (21)$$

The set of values can be from experiment or theory and the index *i* can be *K* or *T*.

The existing ICC calculations differ in their treatment of three major effects: (i) exchange interaction, (ii) presence of

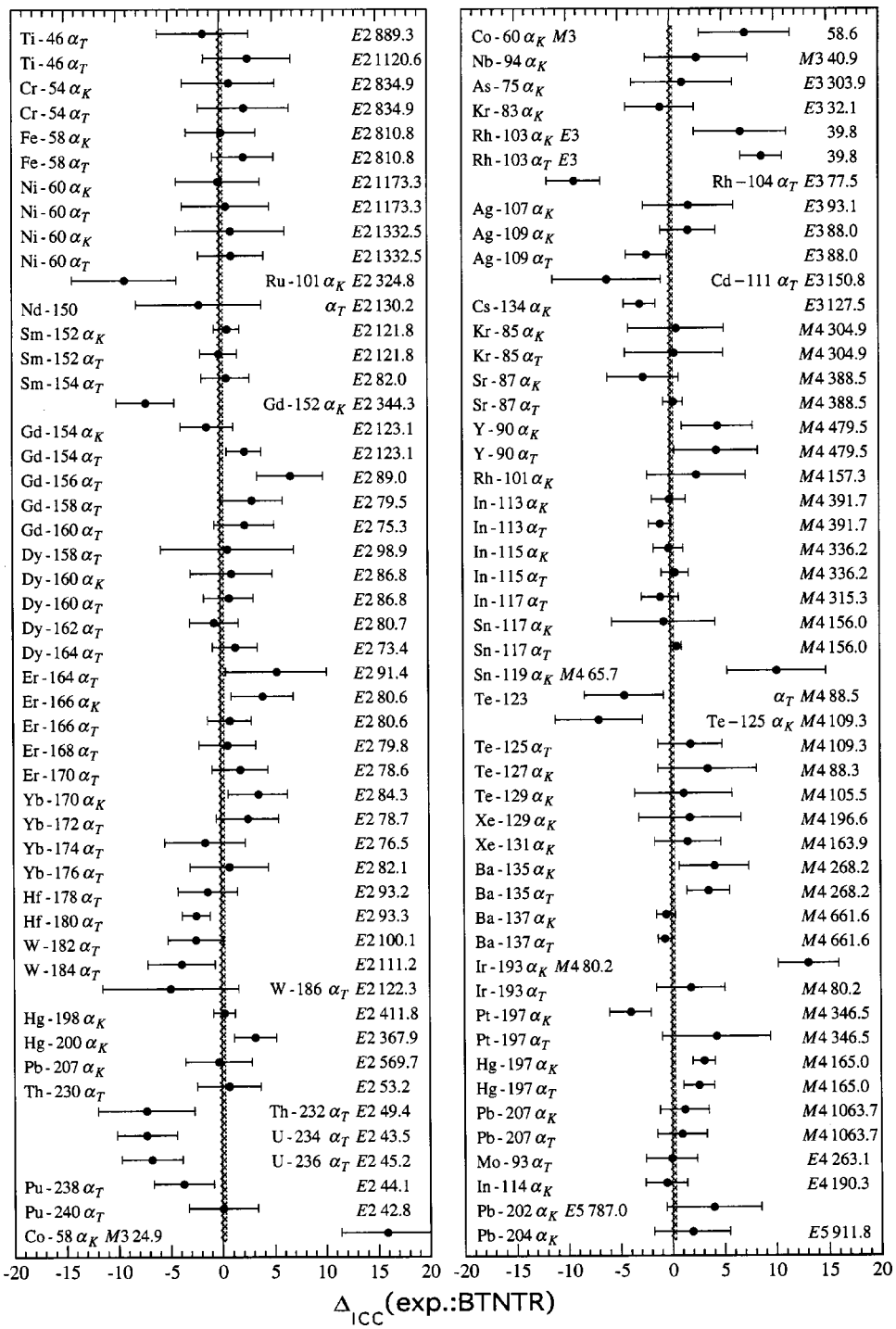

FIG. 6. Comparison between measured conversion coefficients and theoretical Band, Trzhaskovskaya, Nestor, Tikkanen, and Raman (BTNTR) values. See Eq. (21) for the definition of Δ_{ICC}. The data points and error bars are based on the values given in Table VIII. The average difference is $(+0.19\pm0.26)\%$ for these 100 data points.

the hole as a result of electron emission, and (iii) finite size of the nucleus. We discuss the influence of these effects (and also of some other less important effects) next.

1. Exchange interaction

In the HS, RFAP, and BT tables, following a suggestion by Slater [41], the exchange interaction between atomic electrons is taken into account by Eq. (17). There was no coefficient C in the original paper by Slater [41]; that is, $C=1$. Thereafter, Kohn and Sham [42] suggested $C=\frac{2}{3}$. Values between $\frac{2}{3}$ and unity have also appeared in the literature. The HS calculations use $C=\frac{2}{3}$; the RFAP and BT calculations use $C=1$.

In the DF method [used for the BTNTR table and in this work (RNIT)], the exchange terms of DF equations are included exactly, both for the interaction between bound electrons and for the interaction between bound and free electrons. Consequently, the uncertainty in the choice of C is eliminated.

Differences in the treatment of exchange may have a significant influence on the ICCs (and electron binding ener-

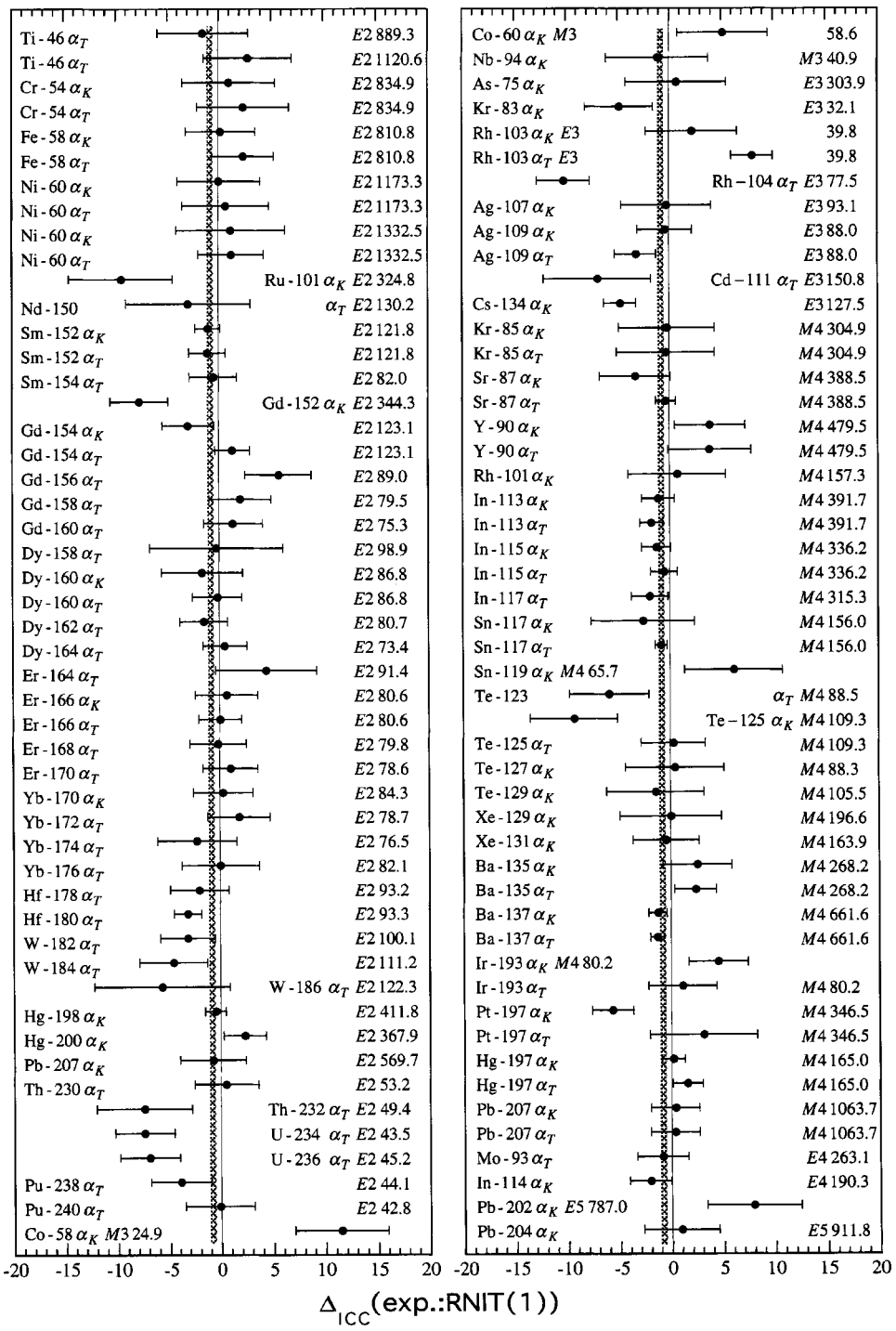

FIG. 7. Comparison between measured conversion coefficients and theoretical Raman, Nestor, Ichihara, and Trzhaskovskaya (this work) [RNIT(1)] values. See Eq. (21) for the definition of Δ_{ICC}. The data points and error bars are based on the values given in Table VIII. The average difference is $(-0.94\pm0.24)\%$ for these 100 data points.

gies). To make quantitative estimates of the corresponding Δ_{ICC}, we have performed calculations with the RHFS [with both $C=1$ (RHFS1) and $C=\frac{2}{3}$ (RHFS$\frac{2}{3}$) in Eq. (17)] and DF methods. All results were obtained with the SC model and the hole was not taken into account. The DF(no-hole) values are the same as the BTNTR values.

Atomic fields calculated by taking screening into account in alternate ways may be considerably different at large distances from the center of an atom. However, these fields are closely related to each other at small distances because the $V_{\rm nucl}$ term [see Eq. (15)] in the potential is very strong at small r. Therefore, the ratio of the electron wave functions obtained in different fields changes very little with r in the atomic region near the nucleus. The square of this ratio is proportional to the ratio of the electron densities near the origin generated in the respective fields. We define two quantities Δ_{ρ_i} and Δ_{ρ_κ} [compare with Eq. (21)] as

$$\Delta_{\rho_i}(\text{set1:set2})=\frac{\rho_i(\text{set1})-\rho_i(\text{set2})}{\rho_i(\text{set2})}\times 100, \qquad (22)$$

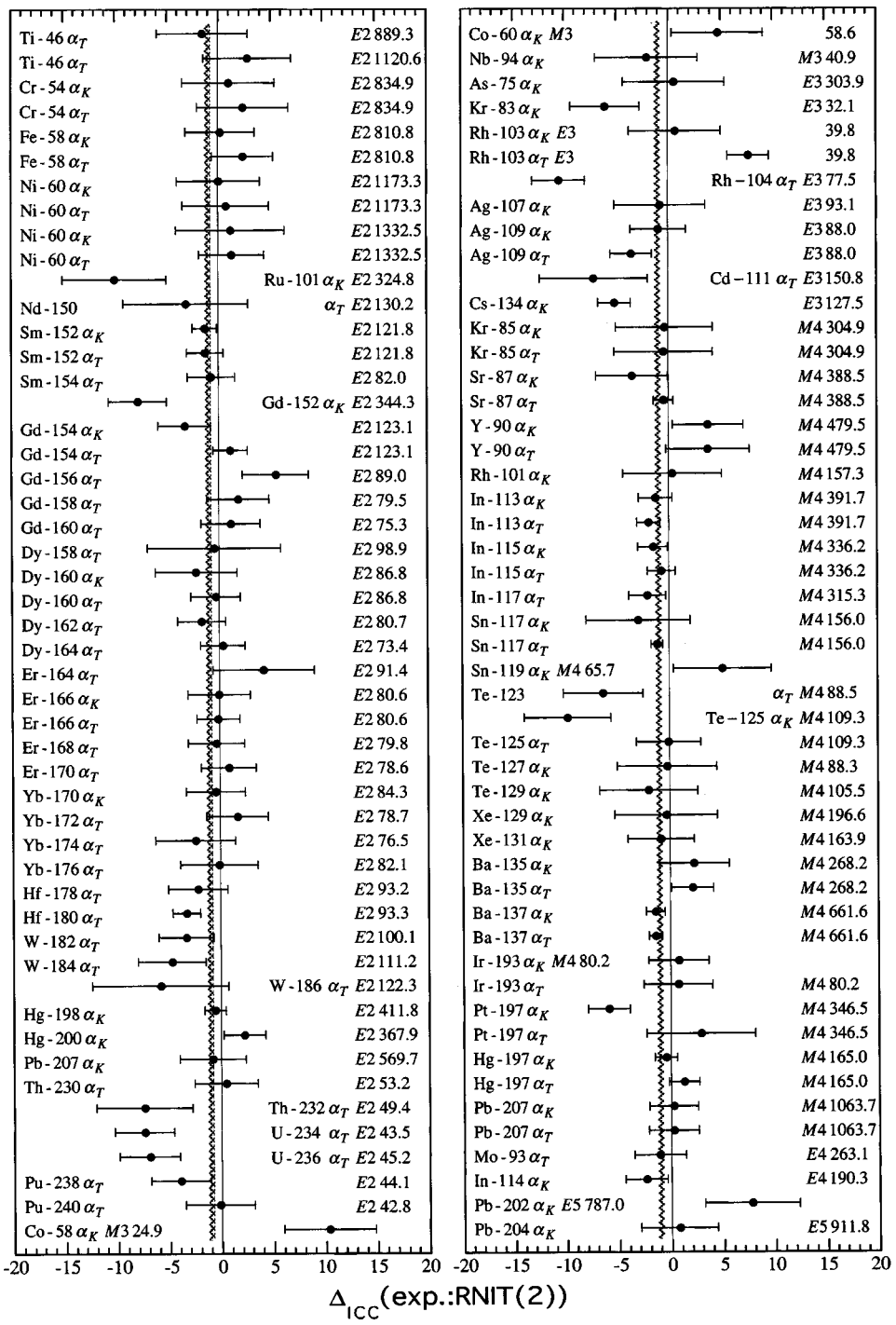

FIG. 8. Comparison between measured conversion coefficients and theoretical Raman, Nestor, Ichihara, and Trzhaskovskaya (this work) [RNIT(2)] values. See Eq. (21) for the definition of Δ_{ICC}. The data points and error bars are based on the values given in Table VIII. The average difference is $(-1.18\pm0.24)\%$ for these 100 data points.

where $\rho_i=\lim_{r\to 0}\rho_i(r)$ is the electron density near the origin for a *bound* electron in the ith atomic shell, and

$$\Delta_{\rho_\kappa}(\mathrm{set1:set2})=\frac{\rho_\kappa(\mathrm{set1})-\rho_\kappa(\mathrm{set2})}{\rho_\kappa(\mathrm{set2})}\times 100, \qquad (23)$$

where $\rho_\kappa=\lim_{r\to 0}\rho_\kappa(r)$ is the electron density near the origin for a *free* electron having a relativistic quantum number κ. If the radius of the formation region of ICC [43] is small and if we take into account the structure of Eqs. (2) and (8), it can be concluded that the changes in ICC calculated in different atomic fields, Δ_{ICC}, should be associated with the changes in electron densities Δ_{ρ_i} and Δ_{ρ_κ}, the latter for that value of κ which makes a main contribution to ICC in Eq. (2).

In Table II we present the Δ_{ICC} and Δ_{ρ_i} results for the 238.6-keV $M1$ transition in $^{212}_{83}\mathrm{Bi}_{129}$ and the 80.6-keV $E2$ transition in $^{166}_{68}\mathrm{Er}_{98}$. (We chose these specific transitions; we could have selected transitions with generic energies just as well.) The Δ_{ICC} values are small for the inner shells, increasing to $\sim 50\%$ for the outer P_1 shell. Table II also shows that the RHFS values with $C=\frac{2}{3}$ are closer to the DF values than

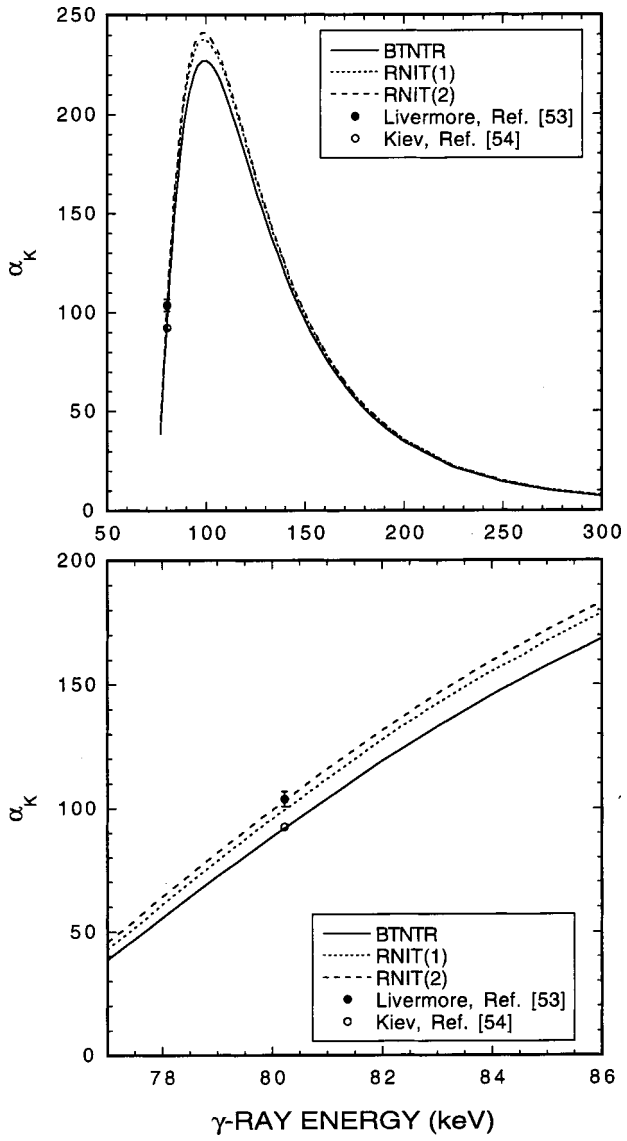

FIG. 9. Behavior of the theoretical α_K values for $M4$ transitions in $^{193}_{77}\mathrm{Ir}_{116}$ as a function of γ-ray energy. The experimental values are for the 80.22-keV $M4$ transition (see Table B of Ref. [32]). The quoted uncertainty in the Kiev value is no bigger than the size of the symbol.

those with $C=1$. Moreover, Δ_{ρ_i} tracks Δ_{ICC} closely. This observation implies that differences in ICC for low-multipolarity ($L\leqslant 2$) and rather high-energy (that is, $E_k > 20$ keV) transitions result mainly from different treatments of the bound electron wave functions.

In Table III we tackle higher-multipolarity ($L\geqslant 3$) transitions in niobium ($Z=41$) and thorium ($Z=90$). Even for the innermost shells, the Δ_{ICC}(RHFS1:BTNTR) values are now quite appreciable; they are as high as $\sim 6\%$ at $E_k=50$ keV with a slight decrease with increasing energy E_k. The Δ_{ρ_i} values (independent of the energy) are no longer close to the Δ_{ICC} values, suggesting that differences in ICC are a result of different treatments of both the bound and continuum wave functions.

Table IV is concerned with very low-energy conversion electrons and outer shells. The values listed there show that the Δ_{ICC}(RHFS:BTNTR) differences are large for low-energy transitions. (This statement is exemplified in Table IV for $E1$, $E3$, and $M3$ transitions; it also applies to low-energy transitions of all multipolarities.) There are also major differences between the Δ_{ICC}(RHFS1:BTNTR) and Δ_{ICC}(RHFS$\frac{2}{3}$:BTNTR) values. Moreover, the Δ_{ICC}(RHFS:BTNTR) values are uncorrelated with the Δ_{ρ_i} values, suggesting that at low E_k the changes in the ICCs for the outer shells result appreciably from changes in the continuum wave functions. The latter changes may be estimated from the Δ_{ρ_κ}(RHFS:BTNTR) values given in Table V for several quantum numbers κ and selected energies. The differences are large when $|\kappa|\geqslant 3$. According to the selection rules [see Eq. (3)], it is these values of κ_f that appear in Eq. (2) for high-multipolarity transitions.

As is evident from Tables II–IV, the exact consideration of the exchange interaction in the calculations of both the discrete and continuum wave functions results in a *decrease* in the ICCs most of the time. The exception (see the negative values in Table IV) is when E_γ is very close to the relevant threshold.

2. Inclusion of the hole

The relationship between the time scale for filling the hole produced in an atomic shell as a result of the emission of a conversion electron and the time it takes for this conversion electron to escape the atom is important in ICC calculations. Most authors make either of two extreme assumptions: (i) the hole is filled instantly and (ii) the hole remains unfilled throughout the period of the removal of the electron.

In the RFAP and BTNTR calculations, the hole is disregarded; that is, the electron wave functions for the initial (bound) and final (continuum) states are both calculated in the self-consistent field (SCF) of a neutral atom. In the HS and BT calculations and in the calculations presented in this work under RNIT(1), the hole is taken into account; that is, the bound wave function is calculated in the SCF of the neutral atom but the continuum wave function is calculated in the SCF of the ion with a vacancy in the shell from which the conversion electron is emitted. (HS do not explicitly state that they include the hole. The fact that they did so emerged subsequently while comparing the HS and BT values [44].)

There exists a second way of taking the hole into account. In the so-called frozen orbital approximation, the continuum wave functions are still calculated in the ion field but this field is not the SCF. Instead, it is constructed using the bound wave functions of the *neutral* atom. The assumption is that there is insufficient time for a rearrangement of the atomic orbitals. We refer to this method as RNIT(2) and ICCs calculated with this method are also presented in this paper. As a general rule, inclusion of the hole by either method increases the ICC values.

On the one hand, from physical considerations, one would argue that the hole should be taken into account. At $E_k>1$ keV, the average time required to fill the hole is significantly longer than the time it takes for an electron of the same energy to escape from an atom. This statement applies to all

TABLE IX. Averaged differences (in %) between experimental and theoretical conversion coefficients for selected sets of data.

Type	α_i	Data	N[a]	$\bar{\Delta}$(exp.:HS)(N)	$\bar{\Delta}$(exp.:RFAP)(N)	$\bar{\Delta}$(exp.:BT)	$\bar{\Delta}$(exp.:BTNTR)	$\bar{\Delta}$(exp.:RNIT(1))	$\bar{\Delta}$(exp.:RNIT(2))
$E2$	α_K	All	14	−2.1±0.7 (10)	−1.5±0.8 (10)	−2.1±0.6	+0.2±0.7	−1.0±0.7	−1.2±0.7
$E2$	α_T	All	35	−2.8±0.5 (29)	−2.9±0.5 (29)	−3.3±0.5	−0.3±0.5	−1.0±0.5	−1.1±0.5
$E2$	α_K, α_T	All	49	−2.6±0.5 (39)	−2.4±0.5 (39)	−2.8±0.4	−0.1±0.4	−1.0±0.4	−1.1±0.4
$E2$	α_K, α_T	$\delta \le 2.5\%$	11	−1.9±0.5	−1.7±0.6	−2.4±0.6	+0.3±0.6	−0.7±0.5	−0.8±0.5
$E2$	α_K, α_T	$\delta > 2.5\%$	38	−3.6±0.7 (28)	−3.3±0.7 (28)	−3.4±0.6	−0.6±0.6	−1.3±0.6	−1.5±0.6
$E3$	α_K, α_T	All	10	−4.6±1.5	−3.6±1.6	−5.1±1.6	−0.9±1.8	−2.6±1.8	−3.0±1.8
$M4$	α_K	All	19	−3.3±0.5	−2.9±0.5	−3.1±0.5	+0.7±0.7	−0.9±0.5	−1.3±0.5
$M4$	α_T	All	15	−2.9±0.3	−2.8±0.3	−3.0±0.3	+0.2±0.4	−0.8±0.3	−1.0±0.3
$M4$	α_K, α_T	All	34	−3.02±0.26	−2.79±0.26	−3.01±0.26	+0.38±0.33	−0.83±0.26	−1.07±0.26
$M4$	α_K, α_T	$\delta \le 2.5\%$	15	−3.03±0.29	−2.87±0.27	−3.02±0.27	+0.21±0.34	−0.92±0.29	−1.12±0.28
$M4$	α_K, α_T	$\delta > 2.5\%$	19	−2.9±0.9	−1.9±0.9	−3.0±0.9	+2.2±1.2	+0.1±0.9	−0.5±0.9
All	α_K	All	45	−3.1±0.4 (37)	−2.4±0.4 (37)	−2.8±0.4	+0.5±0.5	−1.0±0.4	−1.4±0.4
All	α_K	$E_k \le 100$ keV	19	−4.0±0.5 (17)	−2.1±0.6 (17)	−3.4±0.6	+1.7±0.9	−0.9±0.7	−1.6±0.7
All	α_K	$E_k > 100$ keV	26	−2.5±0.6 (20)	−2.6±0.5 (20)	−2.4±0.5	−0.2±0.5	−1.1±0.5	−1.2±0.5
All	α_T	All	55	−3.0±0.4 (49)	−2.9±0.4 (49)	−3.2±0.4	+0.0±0.3	−0.9±0.3	−1.1±0.3
All	α_T	$E_\gamma \le 100$ keV	28	−3.2±0.7	−3.3±0.8	−4.1±0.7	−0.6±0.8	−1.3±0.8	−1.5±0.8
All	α_T	$E_\gamma > 100$ keV	27	−2.9±0.3 (21)	−2.7±0.3 (21)	−2.8±0.3	+0.2±0.3	−0.7±0.3	−0.9±0.3
All	α_K, α_T	All	100	−3.01±0.24 (86)	−2.71±0.24 (86)	−3.04±0.24	+0.19±0.26	−0.94±0.24	−1.18±0.24
All	α_K, α_T	$\delta \le 2.5\%$	31	−2.82±0.28	−2.59±0.27	−2.93±0.28	+0.21±0.30	−0.90±0.29	−1.11±0.29
All	α_K, α_T	$\delta > 2.5\%$	69	−3.8±0.5 (55)	−3.2±0.6 (55)	−3.4±0.5	+0.1±0.6	−1.1±0.5	−1.4±0.5
Unh.[b]	α_K, α_T	All	88	−2.89±0.22 (75)	−2.65±0.23 (75)	−2.92±0.22	+0.25±0.24	−0.84±0.21	−1.06±0.21

[a]Number of data points. In most cases, we can calculate $\bar{\Delta}_{ICC}$(exp.:theory) for the entire set of data points. However, in the case of the HS and RFAP calculations, the averages are, in certain cases, for smaller N values because some of the data points are for nuclei not covered by the Z and L ranges of these calculations.

[b]Unhindered transitions (see also Fig. 2).

elements and all atomic shells [45]. On the other hand, if the hole is taken into account, the electron wave functions computed in different fields for the initial and final states are no longer orthogonal. Nevertheless, ICC calculations can proceed with these wave functions, provided one overlooks the fact that orthogonality is assumed in deriving the ICC expressions.

Presented in Table VI are the differences Δ_{ICC}(hole:no hole) in ICCs calculated by the DF method for $Z=92$ [the "no-hole" case corresponds to BTNTR and the "hole" case to RNIT(1)]. We consider the inner shells, which show the greatest effect. One can see that when E_k is near threshold, the differences can be as much as ~200% for $E4$ and $E5$ transitions. At $E_k=1$ keV, the differences drop to ~15% for $E5$ transitions. Finally at $E_k=100$ keV and higher, the differences do not exceed 3% even in the worst cases.

3. Finite size of the nucleus

The finite size of the nucleus leads to a nonvanishing probability for the penetration of an electron into the nucleus. The transition potential acting on the electron takes on different forms inside and outside the region where the nuclear transition charges and currents responsible for the potential are localized. This difference is referred to as the penetration (or dynamic) effect of the finite nuclear size. This effect is neglected in some calculations. The HS and RFAP tables, for example, are based on the NP model of Rose [6] in which the electron is supposed to be always localized outside the region of nuclear charges and currents. The BT and BTNTR tables, on the other hand, are based on the SC model of Sliv [27] in which the penetration effect is taken into account approximately but consistently for all nuclei and all transitions.

The penetration effect is important if the transition is highly hindered. For unhindered transitions, this effect is not significant for electric transitions but it may be for magnetic transitions—especially for $M1$ transitions converted in the $ns_{1/2}$ shells $(K,L_1,M_1,\ldots)$ (more significant) and the $np_{1/2}$ shells $(L_2,M_2,\ldots)$ (less significant). The ICC(SC) values are always smaller than the ICC(NP) values. Consider, for example, the α_K value for an $M1$ transition with $E_k = 100$ keV. The quantity Δ_{ICC}(NP:SC), calculated with RNIT(1), increases with Z; it is $<1\%$ for $Z=50$, increases to $\sim 5\%$ for $Z=90$, and reaches $\sim 16\%$ for the superheavy $Z=120$ element.

For selected $M4$ transitions, we have compared the ICC(NP) and ICC(SC) values with experiment in Table VII. The ICC(SC) values are favored. Even though the HS [1] and RFAP [2] tables list the ICC(NP) values, it is possible to correct these values for the penetration effect through the use of additional tables [46–48].

4. Other effects

When the transition energy is very close to an ionization threshold, a small difference in the electron binding energy ε_i [see Eq. (12)] has a profound influence on the relevant ICC. For example, a $\sim 2.5\%$ difference in the L_3 binding energy found for fermium $(Z=100)$ between the HS and BT tables translates to a $\sim 21\%$ change in the L_3 ICC for an $E4$ transition at $E_k = 1$ keV. For superheavy elements, the ICCs from the DF calculations [19] and the recent Ryšavý and Dragoun [49] RHFS calculations differ at low E_k not only because the methods of treating exchange are different but also because the eigenvalues (used in lieu of the experimental binding energies) are different. If the energy E_k is not too low (greater than several tens of keV), variations in ε_i lead to insignificant effects $(\leqslant 0.5\%)$ on ICCs. In this work, we need to be concerned only in the case of the 80.22-keV $M4$ transition in $^{193}_{77}$Ir. For the K shell, the E_k value is 4.1 keV in this case. Fortunately, the K-shell binding energy, 76.110 keV, for iridium used in the BT, BTNTR, and RNIT calculations is virtually the same as 76.111 keV used in the HS and RFAP calculations.

There is a resonance effect that might influence the ICCs in some special cases. In the cases of the L_1 curves for $E2$-$E5$ transitions in light and medium elements, there are pronounced resonancelike structures below 100 keV (see, for example, Fig. 2 of Ref. [2] or Fig. 1 of Ref. [19]). They are a result of cancellations suffered by the leading matrix element. The positions of the resonance minima are given by

$$E_\gamma(\mathrm{keV}) \approx \frac{(L-1)Z^2}{200}, \tag{24}$$

corresponding to the energies at which the L_1 conversion goes to zero in a nonrelativistic calculations in a Coulomb field [50]. This resonance-type behavior occurs also for the higher $s_{1/2}$ shells and affects the $M_1,N_1,\ldots$ ICCs. This effect is not a problem if the ICC is calculated for a specific energy (with a computer code corresponding to a particular method) or if the transition energy is far removed from a resonance. It could become a problem if the ICC is obtained through interpolation of published values and if the latter are not detailed enough to delineate the resonance.

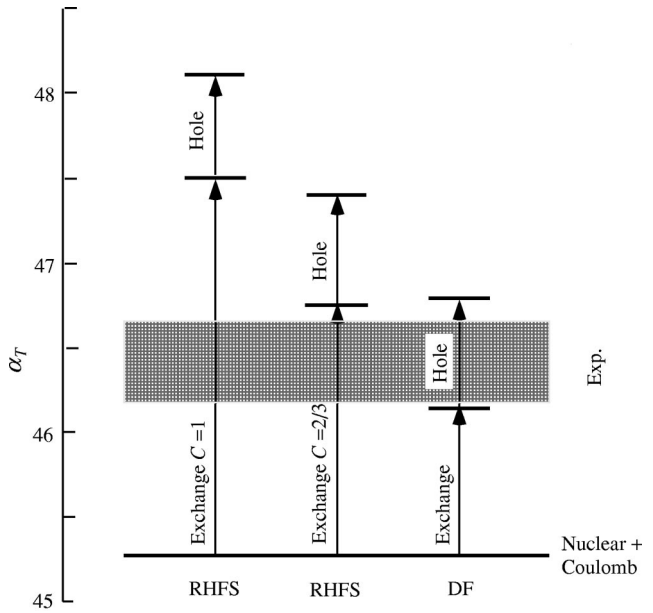

FIG. 10. Decomposition of the calculated ICC into contributions from (i) interaction of the electron with the nucleus + Coulomb interaction between electrons, (ii) the electron exchange interaction, and (iii) the influence of the hole resulting from the ejection of the conversion electron. The calculations are for the 156.02-keV $M4$ transition in $^{117}_{50}\mathrm{Sn}_{67}$. The experimental value is from Ref. [8].

For magnetic transitions in heavy elements, there are differences between ICCs given in the HS and BT tables and those given in the RFAP table—differences that cannot be explained by differing physical assumptions. For $M1$ transitions, these differences can reach $\sim 30\%$ for the L_2 shell [51]. Moreover, the analysis carried out by Dragoun and Ryšavý [52] shows that serious errors (as opposed to expected differences) exist in the RFAP total ICCs for low-energy transitions. However, these errors do not significantly affect the global comparisons made in this work.

V. COMPARISON BETWEEN EXPERIMENT AND THEORY

We are now in a position to make detailed comparisons between the experimental and theoretical ICCs. In Table VIII, we have listed the adopted experimental ICCs carried over from Table B of Ref. [32]. There are some gaps in the HS and RFAP columns because the relevant ICCs lie outside the Z or L ranges of these calculations (see Table I). We have also listed in Table VIII the corresponding theoretical values from six different calculations. The quantities Δ_{ICC}(expt:theory) for each of these six calculations are plotted in Figs. 3–8. In general, we are not interested in pursuing the comparison between the experimental and theoretical ICCs on a case-by-case basis. Instead, we are interested in obtaining a ''global'' or ''averaged'' view of the level of agreement.

If $x_1 \pm \delta x_1$, $x_2 \pm \delta x_2, \ldots x_n \pm \delta x_n$ are n independent measurements, δx_i being the uncertainty in x_i, then the

weighted average (weighted by the inverse square of the uncertainty) is given by $\overline{x} \pm \overline{\delta x}$, where

$$\overline{x} = W \sum_1^n x_i/(\delta x_i)^2, \tag{25a}$$

$$W = 1 \Big/ \sum_1^n (\delta x_i)^{-2}, \tag{25b}$$

and $\overline{\delta x}$ is the larger of

$$(W)^{1/2} \tag{26a}$$

$$\text{and} \quad \left[W \sum_1^n (\Delta x_i)^{-2} (\overline{x} - x_i)^2/(n-1) \right]^{1/2}. \tag{26b}$$

The shaded lines in Figs. 3–8 are the weighted average values given by these expressions.

The average $\overline{\Delta}_{\rm ICC}$(expt:theory) values for the HS, RFAP, and BT calculations (see Figs. 3, 4, and 5) are $(-3.01 \pm 0.24)\%$, $(-2.71 \pm 0.24)\%$, and $(-3.04 \pm 0.24)\%$, respectively. These three calculations are based on the RHFS method and there can be no doubt that they overpredict the ICCs in our database by $\sim 3\%$.

The average $\overline{\Delta}_{\rm ICC}$(expt:theory) values for the BTNTR, RNIT(1), and RNIT(2) calculations (see Figs. 6, 7, and 8) are $(+0.19 \pm 0.26)\%$, $(-0.94 \pm 0.24)\%$, and $(-1.18 \pm 0.24)\%$, respectively. These three calculations are based on the DF method. The DF values are, on average, 2–3 % lower than the RHFS values and, therefore, in much better agreement with experiment.

Even though the best overall agreement between experiment and theory, $\overline{\Delta}_{\rm ICC}$(expt:theory) $= (+0.19 \pm 0.26)\%$, was found with the BTNTR (no-hole) values, we believe on physical grounds that the ''correct'' theory should take the hole into account. The two methods of accomplishing this purpose [RNIT(1) and RNIT(2)] result in theoretical values that are, on average, $\sim 1\%$ larger than experiment.

Differences between various theoretical ICCs are significant when the transition energy is close to the binding energy. Of all the transitions studied in this work, the α_K values for the 80.22-keV $M4$ transition in ^{193}Ir show the largest spread in the theoretical values. This transition energy is close to the iridium ($Z=77$) K-shell binding energy of 76.11 keV. The lowest value, $\alpha_K = 91.93$, is given by BTNTR; the highest value, $\alpha_K = 110.3$ by HS (see Table VIII). In Fig. 9, we show the behavior of the theoretical α_K values for ^{193}Ir as a function of the γ-ray energy. At 80.22 keV, the BTNTR, RNIT(1), and RNIT(2) values are, respectively, 91.93, 99.47, and 103.2. Here is a case where a reliable α_K measurement would have provided definite theoretical clues. Unfortunately, the two reported experimental α_K values, 104 ± 3 (Livermore) [53] and 92.6 ± 0.9 (Kiev) [54], differ by $\sim 10\%$. The Livermore value favors the RNIT(hole) value while the Kiev value is close to the BTNTR(no-hole) value.

In addition to the obtaining global average $\overline{\Delta}_{\rm ICC}$(expt:theory) values for ~ 100 ICCs, it is possible to divide the database into various subgroups and study their average behaviors, as we have done in Table IX. This study confirms our basic conclusion that, on average, the RHFS (HS, RFAP, and BT) values are $\sim 3\%$ larger than experiment while the DF [BTNTR, RNIT(1), and RNIT(2)] values are only 0–1 % larger than experiment. The subgroup of α_K, $E_k \leqslant 100$ keV (see row 13 of Table IX) is most sensitive to physical assumptions made in the theory. This set of 19 values is reproduced best by RNIT(1) except that the theoretical values are, on average, $\sim 1\%$ larger than experiment.

There are ten data points in the $E3$ subgroup (see row 6 of Table IX). The theoretical ICCs for these transitions are, on average, about 1–5 % larger than experiment. We know from Fig. 2 and earlier discussion in Sec. III that we need to consider the possibility of $M4$ admixtures in these transitions. However, any $M4$ admixtures would serve to only further widen the discrepancy between theory and experiment. Therefore, at least for the purposes of the current work, it is appropriate to treat these transitions as pure $E3$. Alternatively, had we omitted the hindered transitions (see Fig. 2) altogether from our considerations, our main conclusions would not be affected significantly (see last row of Table IX).

To understand which effect is responsible for the 2–3 % reduction of the DF values from the RHFS values, we show in Fig. 10 an analysis of the theoretical α_T values for the 156.02-keV $M4$ transition in ^{117}Sn. The influence of the hole is similar in the RHFS and DF calculations. It is the influence of the exchange term that is markedly different and mainly responsible for the reduction in the ICC. The benchmark experimental value [8] $\alpha_T = 46.40$, with a conservatively estimated uncertainty of ± 0.25, lies approximately midway between the theoretical values of 46.14 (BTNTR) and 46.80 [RNIT(1)].

VI. CONCLUSIONS

During the 1960s, it was generally believed that the theoretical ICCs were accurate at the 5–10 % level. In 1973, Raman *et al.* [8] showed that the HS (RHFS) ICCs were more accurate than generally believed except that they were systematically 2–3 % larger than experiment. During the 1980s, it became clear [13–18] that this systematic discrepancy was a common problem that afflicted all RHFS calculations.

A computer code [20–22] became available in the late 1980's in which significant improvements were made in the treatment of the exchange interaction. Calculations made with this code show that the use of the Slater exchange term in the RHFS method results in an overestimation of ICCs even after the influence of this term is reduced to $\frac{2}{3}$.

During the past five decades, a large number of measurements have been carried out for 77 transitions throughout the periodic table from which one can select 100 ICCs that have experimental uncertainties $\leqslant 5\%$. The DF calculations are able to reproduce the experimental values, on average, at the 0–1 % level. This ability is proof of a significant improvement of ICC theory.

Further progress in this field requires additional measurements carried out with better than 1% accuracy. Currently

there are only five ICCs known (see Table B of Ref. [32]) to better than 1% accuracy (α_K in ^{137}Ba and ^{198}Hg, and α_T in ^{87}Sr, ^{117}Sn, and ^{137}Ba). The theoretical ICCs become very sensitive to physical assumptions when the transition energy is very close to the binding energy. Suppose we want to study the influence of the hole by means of a new experiment designed to measure ICC with an uncertainty of $\pm 2\%$. In the current database (see Table VIII), there are only three transitions ($E3$ in ^{83}Kr and ^{103}Rh and $M4$ in ^{193}Ir) for which the BTNTR (no-hole) and RNIT(1) (hole) α_K values differ by more than twice this uncertainty. The two measured values for the most promising case (^{193}Ir) differ by $\sim 10\%$. We plan to remeasure this value.

Accurate experimental subshell ratios are more numerous than accurate experimental α_K and α_T values. We are in the process of examining how well the subshell ratios are reproduced by the theoretical calculations.

There may exist a residual $\sim 1\%$ discrepancy between the experimental and theoretical (RNIT) ICC values. The latter are slight overestimates. This systematic difference may be associated with higher-order effects (such as electron correlations, vacuum polarization, etc.) that are neglected in the calculations. While taking the hole into account, it is also desirable to orthogonalize the wave functions at each step of the self-consistent field calculations. This procedure is currently not followed in the ICC calculations discussed in this paper.

ACKNOWLEDGMENTS

This work was sponsored partly by the Office of High Energy and Nuclear Physics, U.S. Department of Energy under Contract No. DE-AC05-00OR22725 with UT-Battelle, LLC and partly by the Russian Foundation for Basic Research under Grant No. 02-02-17117 with the Petersburg Nuclear Physics Institute. One of us (M.B.T.) is grateful to the Joint Institute for Heavy-Ion Research for arranging her assignments to Oak Ridge and to ORNL for its hospitality. We thank I. M. Band for making available the DF code for use at Oak Ridge and M. J. Martin for critically reading this paper.

[1] R.S. Hager and E.C. Seltzer, Nucl. Data, Sect. A **A4**, 1 (1968).
[2] F. Rösel, H.M. Fries, K. Alder, and H.C. Pauli, At. Data Nucl. Data Tables **21**, 91 (1978).
[3] I.M. Band and M.B. Trzhaskovskaya, Tables of Gamma Ray Internal Conversion Coefficients for K, L and M Shells, $10 \leqslant Z \leqslant 104$, Leningrad Nuclear Physics Institute report, 1978 (in Russian).
[4] M. Ryšavý and O. Dragoun, J. Phys. G **26**, 1859 (2000).
[5] *Proceedings of the International Conference on the Internal Conversion Process, Nashville, Tennessee, 1965*, edited by J.H. Hamilton (Academic, New York, 1966).
[6] M.E. Rose, in *Beta- and Gamma-Ray Spectroscopy*, edited by K. Siegbahn (North-Holland, Amsterdam, 1955), p. 905; *Internal Conversion Coefficients* (North-Holland, Amsterdam, 1958); in *Proceedings of the International Conference on the Internal Conversion Process* (Ref. [5]), p. 15.
[7] L.A. Sliv and I.M. Band, *Tables of Gamma-Ray Internal Conversion Coefficients, Part I: K Shell* (Academy of Sciences USSR, Leningrad, 1956); *Tables of Gamma-Ray Internal Conversion Coefficients, Part II: L Shell* (Academy of Sciences USSR, Leningrad, 1958); see also in *Gamma Rays*, edited by L.A. Sliv (Academy of Sciences USSR, Leningrad, 1961), p. 318 (in Russian); see also in *Alpha-, Beta-, and Gamma-Ray Spectroscopy*, edited by K. Siegbahn (North-Holland, Amsterdam, 1965), p. 1639.
[8] S. Raman, T.A. Walkiewicz, R. Gunnink, and B. Martin, Phys. Rev. C **7**, 2531 (1973).
[9] J.L. Campbell and B. Martin, Z. Phys. A **274**, 9 (1975).
[10] I.M. Band and M.A. Listengarten, Izv. Akad. Nauk SSSR, Ser. Fiz. **38**, 1588 (1974) [Bull. Acad. Sci. USSR, Phys. Ser. (Engl. Transl.) **38**, 24 (1974)].
[11] O. Dragoun, V. Brabec, M. Ryšavý, J. Plch, and J. Zderadička, Z. Phys. A **279**, 107 (1976).
[12] S. Raman, C.H. Malarkey, W.T. Milner, C.W. Nestor, Jr., and P.H. Stelson, At. Data Nucl. Data Tables **36**, 1 (1987).
[13] Zs. Németh and Á. Veres, Phys. Rev. C **35**, 2294 (1987).
[14] Zs. Németh, Á. Veres, T. Sekine, and K. Yoshihara, in *Proceedings of the International Conference on Nuclear Data for Science and Technology, Mito, Japan, 1988*, edited by S. Igarasi (Saikon, Tokyo, 1988), p. 849.
[15] Zs. Németh and Á. Veres, Nucl. Instrum. Methods Phys. Res. A **286**, 601 (1990).
[16] I.M. Band, M.A. Listengarten, and M.B. Trzhaskovskaya, Izv. Akad. Nauk SSSR, Ser. Fiz. **53**, 910 (1989) [Bull. Acad. Sci. USSR, Phys. Ser. (Engl. Transl.) **53**, 85 (1989)].
[17] I.M. Band, M.A. Listengarten, and M.B. Trzhaskovskaya, Izv. Akad. Nauk SSSR, Ser. Fiz. **54**, 15 (1990) [Bull. Acad. Sci. USSR, Phys. Ser. (Engl. Transl.) **54**, 14 (1990)].
[18] I.M. Band and M.B. Trzhaskovskaya, Izv. Akad. Nauk SSSR, Ser. Fiz. **55**, 2141 (1991) [Bull. Acad. Sci. USSR, Phys. Ser. (Engl. Transl.) **55**, 59 (1991)].
[19] I.M. Band, M.B. Trzhaskovskaya, C.W. Nestor, Jr., P. Tikkanen, and S. Raman, At. Data Nucl. Data Tables **81**, 1 (2002).
[20] I. M. Band, M. A. Listengarten, M. B. Trzhaskovskaya, and V. I. Fomichev, Computer Program Complex RAINE I–IV, Leningrad Nuclear Physics Institute Reports LNPI-289, 1976; LNPI-298, 1977; LNPI-299, 1977; LNPI-300, 1977.
[21] I.M. Band and V.I. Fomichev, Leningrad Nuclear Physics Institute Report LNPI-498, 1979.
[22] I.M. Band, M.A. Listengarten, and M.B. Trzhaskovskaya, Leningrad Nuclear Physics Institute Report LNPI-1479, 1989.
[23] I.M. Band and M.B. Trzhaskovskaya, At. Data Nucl. Data Tables **55**, 43 (1993).
[24] O. Dragoun, M. Ryšavý, F. Bečvář, and V. Brabec, Czech. J. Phys., Sect. B **31**, 246 (1981).
[25] Zs. Németh, Nucl. Instrum. Methods Phys. Res. A **312**, 296 (1992).
[26] N. Coursol, V.M. Gorozhankin, E.A. Yakushev, C. Briançon,

and Vylov, Appl. Radiat. Isot. **52**, 557 (2000).
[27] L.A. Sliv, Z. Phys. **21**, 770 (1951).
[28] R.P. Feynman, R.B. Leighton, and M. Sands, *The Feynman Lectures on Physics* (Addison-Wesley, Reading, MA, 1964), Vol. 1, p. 1.
[29] J.H. Hamilton, in *The Electromagnetic Interaction in Nuclear Spectroscopy,* edited by W.D. Hamilton (North-Holland, Amsterdam, 1975), p. 441.
[30] P.H. Stelson, in *Proceedings of the International Conference on the Internal Conversion Process* (Ref. [5]), p. 213.
[31] S.C. Pancholi, Nucl. Phys. **67**, 203 (1965).
[32] See EPAPS Document No. E-PRVCAN-66-049210 for the electronic addendum to this paper. It includes Table A, Table B, and references. A direct link to this document may be found in the online article's homepage (http://www.aip.org/pubservs/epaps.html) or from ftp.aip.org in the directory/epaps/. See the EPAPS homepage for more information.
[33] I.M. Band, M.A. Listengarten, and A.P. Feresin, *Anomalies in Gamma-Ray Internal Conversion Coefficients* (Nauka, Leningrad, 1976) (in Russian).
[34] J.A. Bearden and A.F. Burr, Rev. Mod. Phys. **39**, 125 (1967).
[35] K. Siegbahn, C. Nordling, A. Fahlman, R. Nordberg, K. Hamrin, J. Hedman, C. Johansson, T. Bergmark, S.-E. Karlsson, I. Lindgren, and B. Lindberg, *ESCA: Atomic, Molecular, and Solid State Structure Studied by Means of Electron Spectroscopy* (Almqvist and Wiksells, Uppsala, 1967).
[36] W. Lotz, J. Opt. Soc. Am. **60**, 206 (1970).
[37] M.S. Freedman, F.T. Porter, and J.B. Mann, Phys. Rev. Lett. **28**, 711 (1972).
[38] C.C. Lu, T.A. Carlson, F.B. Malik, T.C. Tucker, and C.W. Nestor, Jr., At. Data **3**, 1 (1971).
[39] O. Dragoun, H.C. Pauli, and F. Schmutzler, Nucl. Data, Sect. A **6**, 235 (1969).
[40] O. Dragoun, Z. Plajner, and F. Schmutzler, Nucl. Data Tables **9**, 119 (1971).
[41] J.C. Slater, Phys. Rev. **81**, 385 (1951).
[42] W. Kohn and L.J. Sham, Phys. Rev. **140**, A1133 (1965).
[43] I.M. Band, L.A. Sliv, and M.B. Trzhaskovskaya, Nucl. Phys. **A156**, 170 (1970).
[44] I.M. Band, M.A. Listengarten, and M.B. Trzhaskovskaya, Izv. Akad. Nauk SSSR, Ser. Fiz. **41**, 2035 (1977) [Bull. Acad. Sci. USSR, Phys. Ser. (Engl. Transl.) **41**, 39 (1977)].
[45] M.A. Listengarten and V.O. Sergeev, in *Proceedings of the IX Workshop on Nuclear Physics, Bukhara, Uzbekistan, 1979*, edited by V.P. Prikhodceva (Nauka, Leningrad, 1981), p. 39 (in Russian).
[46] R.S. Hager and E.C. Seltzer, Nucl. Data, Sect. A **6**, 1 (1969).
[47] E. Browne and F. Femenia, Nucl. Data Tables **10**, 81 (1971).
[48] D. Krpič, I. Aničin, and R. Vukanović, Nucl. Data Tables **11**, 553 (1973).
[49] M. Ryšavý and O. Dragoun, At. Data Nucl. Data Tables **78**, 129 (2001).
[50] E.L. Church and J.E. Monahan, Phys. Rev. **98**, 718 (1955).
[51] I.M. Band and M.B. Trzhaskovskaya, Izv. Akad. Nauk SSSR, Ser. Fiz. **56**, 1745 (1992) [Bull. Acad. Sci. USSR, Phys. Ser. (Engl. Transl.) **56**, 1745 (1992)].
[52] O. Dragoun and M. Ryšavý, J. Phys. G **18**, 1991 (1992).
[53] M. Lindner, R. Gunnink, and R.J. Nagle, Phys. Rev. C **36**, 1132 (1987).
[54] V.A. Zheltonozhsky, P.N. Muzalev, A.F. Novgorodov, and M.A. Ukhin, Zh. Éksp. Teor. Fiz. **91**, 32 (1988) [Sov. Phys. JETP **67**, 16 (1988)].